Bull. Disas. Prev. Res. Inst., Kyoto Univ., Vol. 39, Part 3, No. 340, September, 1989

A Laboratory Experiment on the Evaporation from Bare Land with an Underlying Unrestricted Water Table

By Yasuo Ishihara and Eiichi Shimojima

(Manuscript received on July 3, 1989)

Abstract

To elucidate the evaporation process from bare land, such as a desert with an underlying unrestricted groundwater-table, a laboratory evaporation experiment was carried out by continuously applying a turbulent airflow with constant speed, temperature and humidity to several kinds of porous material layers: fine sand, uniform glass bead and Akadama-soil. Through examination of the data obtained, the following conclusions have been reached: 1) Turbulent airflow affects the evaporation rate, E, and the degree of this effect becomes small with the increase in the water table depth, z_w, and the increase in the depth of evaporating front, z_e. The degree of the effect becomes larger as pore-size of the porous material layer increases in size; 2) While turbulence has a great effect on water vapour transfer in the porous material layer, the relation between E/u_* and z_w is unique regardless of wind speeds, where u_* is the friction velocity; 3) In time-courses of evaporation rate and change in water table depth, a characteristic change appears over any given duration. In the case of the sand, and of the Akadama-soil which displays a double pore structure (macropore and micropore) in the second stage, it is satisfied that $E=const.\exp(-const.\ t)$ and $z_w=const.\exp(const.\ t)+const.$ Particularly for the soil, these behaviours persist for quite a long time because the evaporating front stays near the exposed surface of the soil layer; 4) After a significant time has elapsed (i.e. in the third stage), in the cases of the sand and the glass beads of relatively small particle-diameter (on the order of 1 mm), the result that $E=const./[t+const.]^{1/2}$ and z_w or $z_e=const.[t+const.]^{1/2}+const.$ is satisfied.

1. Introduction

Evaporation from bare land is a phenomenon in which the aqueous content of the soil is directly transferred into the atmosphere from the ground surface in the gaseous phase, due to vaporization. This phenomenon is one of the important elements in the hydrologic cycle and in practice plays a key role in the problems of water resources and land use (e.g., Sadler & Cox (1986)[1]), especially in semi-arid and arid regions.

The evaporation process consists of two major sub-processes: The first is the movement of liquid water in the soil (porous media) in relation to the occurrence of the evaporation. When the evaporation occurs below the surface, the water vapour must move upwards towards the surface through the soil. The second is the transfer into the atmosphere of both the water vapour which has moved up to the surface as well as that liquid water which vaporizes at the surface. A turbulent boundary layer

often develops above the surface. These sub-processes mutually interact throughout the land surface, and each affects the other in complicated manner under thermal conditions such as solar radiation. In order to clarify the evaporation mechanism in and over the bare land, it is necessary in the analysis to treat the evaporation field as an atmosphere-land continuum.

The evaporation phenomenon is interdisciplinary, involving research in soil physics, meteorology, hydrology, environmental engineering, etc. For example, the transfer mechanism of the water vapour and the heat in the atmosphere, and in the soil, have been studied in micro-meteorology (Brutsaert (1982)[2]) and in soil physics (Hillel (1980)[3]), respectively. Based on a recent and remarkable progress in employment of the computer, there is a numerical simulation wherein a numerical solution of a set of complicate fundamental equations for water and heat in the atmosphere-land continuum is undertaken (Camillo et al (1983)[4], Bristow et al (1986)[5], Kuzuha et al (1988)[6], Ishihara et al (1989)[7]). Its methodology is powerful, although it is still not certain whether the phenomena near the ground surface have been properly incorporated into the fundamental equations.

This paper describes a laboratory experiment on the evaporation from bare land, such as a desert, with an underlying unrestricted groundwater table. The experiment was carried out by continuously applying a turbulent airflow with an averaged constant speed, temperature, and humidity to the exposed surface of several kinds of porous material layer employing sand, glass beads and Akadama-soil, in a windtunnel. The purpose of this research is to elucidate the evaporation process, paying particular attention to the effect of turbulent wind on evaporation.

2. Materials and Method

A uniform porous material layer with a width of 34 cm, length of 94 cm, and depth of 67 cm was set up in a transparent, rectangular prism box, and was installed on a balance resembling a weighing lysimeter.

On the porous material layer, a straight wind tunnel with a cross-section of 40 cm $\times$ 40 cm was set. The wind tunnel is a Göttingen type and wind speed, temperature, and humidity can be regulated. The exposed surface of the porous material layer serves as part of a permeable bottom plate of the wind tunnel.

Porous cups and thermocouples were horizontally inserted into the porous material layer at suitable locations, through the side wall of the box. The sensing bar-tips of the thermocouples were located in the central part of the porous material layer. Water pressure in the porous material layer was measured by a manometer connected to the porous cups.

The porous materials employed were two kinds of sand, designated as Sand K-5, and Sand K-6, three kinds of glass bead, designated as Bead-1, Bead-2, and Bead-3, and Akadama-soil. Sand K-5 and Sand K-6 were of fairly uniform in particle-size, with mean diameters of 0.45 mm and 0.22 mm, respectively. The glass beads were uniform with diameters of 12 mm for Bead-1, 5 mm for Bead-2, and 2 mm for Bead-3.

The particle-size of Akadama-soil ranges from about 1 to about 6 mm, with a mean diameter of 3 mm. The soil has a double-pore structure. One is in the massive porous materials, and the other is formed among the massive porous materials, corresponding to each the so-called micropore and macropore. The air-entry values for Sand K-6, Sand K-5, and Akadama-soil are -12 cmH_2O, -5 cmH_2O and zero, respectively. It is zero for Bead-1, -1 cmH_2O for Bead-2 and -2 mmH_2O for Bead-3. The field capacity is 0.03 for Sand K-6, 0.04 for Sand K-5, and 0.15 for Akadama-soil, in volumetric water content, θ.

In the experiment, the unrestricted condition of the groundwater table was achieved as follows. Before starting an evaporation experiment, fresh water was slowly supplied from below the porous material layer till free water appeared at the exposed surface of the layer. The saturated porous material layer was allowed to reach thermal equilibrium with the ambient temperature over two days in a laboratory maintained at near 25°C. The experiment was then run by continuously applying a turbulent airflow to the surface through the windtunnel. The airflow was about 25.5°C in temperature, about 40% in relative humidity, and maintained at averaged constant speed. The wind velocities were varied in several magnitude except in the case of Akadama-soil. For Sand K-5, and the three glass beads the mean velocity of the airflow in the windtunnel, U, was 290 cm/s and 150 cm/s. For Sand K-6, $U=$ 295 cm/s, 285 cm/s, 215 cm/s, 150 cm/s and 67 cm/s. For Akadama-soil, $U=$ 290 cm/s was unvaryingly applied. The duration of each experiment ranged from approximately one to three months.

During the experiment, neither water supply into the porous material layer, nor artificial drainage from the layer, was undertaken. Furthermore, incident heat, e.g. short wave radiation simulating the sun was not applied to the exposed surface.

3. Experimental Results

(1) The case of Sand K-5

1) *Evaporation rate*

Changes in the evaporation rate, E, for Sand K-5, are plotted in a logarithmic scale against time, t, in **Fig. 1**, where closed and open circles are used for the applied mean wind velocities, $U=290$ cm/s and $U=150$ cm/s, respectively. The following can be reduced from this figure. The evaporation rate decreases rapidly immediately after the onset of the experiment and its decreasing rate becomes small at a certain time (stage-1). Subsequently, the evaporation rate seems to decrease following the broken line drawn in the figure for a certain duration, i.e., approximately $t=100$–200 h for $U=290$ cm/s, and about $t=150$–300 h for $U=150$ cm/s (stage-2). Finally, E begins to decrease quite slowly with time (stage-3). The change in stage-2 indicates that the evaporation rate decreases exponentially with time. The exponential decay coefficient, f_*, becomes larger with increasing wind speed, but the degree of the difference is not necessarily large (see **Table 2**). The evaporation rate for the stronger wind is at first larger than that for the weaker one, but this relation reverses

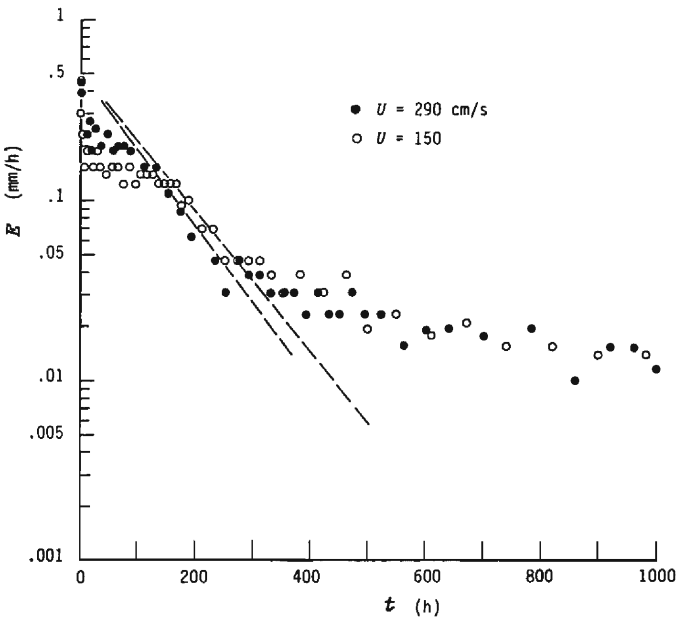

Fig. 1. Changes in the evaporation rate with time in the case of Sand K-5.

as t increases, with the degree of the difference becoming small.

Cumulative evaporation was always larger at the higher wind velocities.

2) *Water table depth*

Time-courses of the water table depth, $z_w(t)$, corresponding to **Fig. 1**, are shown in **Fig. 2**. Measurement of the water pressure suggested that the water table was essentially horizontal. At the beginning of the experiment the water table fell rapidly, but at a rate which decreases with time. The rapid fall at the early stage is evidently based on the effect of the capillary rise of the sand (capillary fringe) and much evapo-

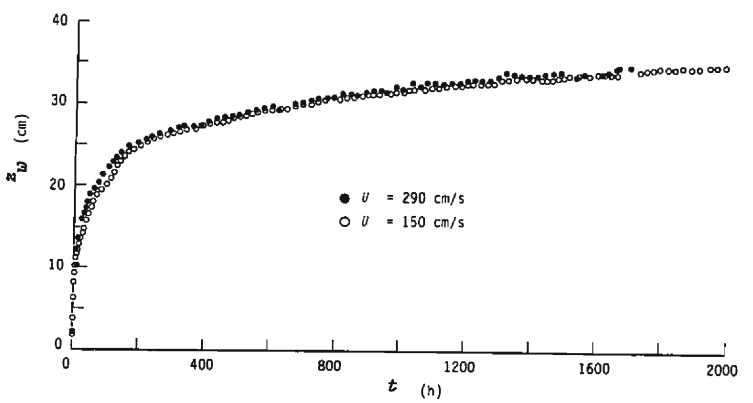

Fig. 2. Changes in the water table depth with time, corresponding to Fig. 1.

ration. The water table is always deeper for the stronger wind, over the duration of the experiment, but the differences in the increase in depth of the water table seem to have become very small after a significant amount of time has elapsed.

3) *Water content profile*

Through measurement of the water pressure in the sand layer, the water content profile reveals the following. After much time has elapsed, the profile always satisfies the so-called equilibrium condition very accurately except near the sand surface, so that from the initial water content condition of the sand layer, the profile can be represented by the boundary soil-water retention curve under drying. We denote this as the BDSR-curve.

Fig. 3 shows water content profiles in volumetric water content (θ), near the sand surface at the end of experiment, i.e. $t=2200$ h (about 3 months), where the wind velocity was $U=150$ cm/s. Solid lines indicate the observed data which were derived from measurements of samples of sand taken from different depths at three locations. The broken line represents the equilibrium water content profile above the water table. The solid lines separate sharply from the broken line above 5 cm depth. The observed water content above that depth decreases first in an upward convex curve, and then with decreasing depth, an inflexion occurs and the convex curve faces downward. The water content tends to nearly constant value, θ_r. Water content at the separating point is $\theta=0.07$. The value of θ_r is 0.02, which is smaller than the field capacity ($\theta_f=0.05$). Therefore, we can say that the observed water content profile at $t=$ 2200 h is consistent with the BDSR-curve below the 5 cm depth, and that the sand above that depth becomes very desiccated via a steep slope of the profile, which cannot be represented by the BDSR-curve. The appearance of the inflexion point is caused

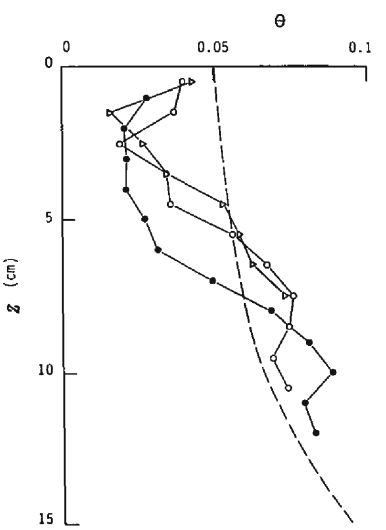

Fig. 3. Water content profiles near the surface of Sand K-5 layer at $t=2200$ h under the condition that $U=150$ cm/s.

by a functional characteristic of moisture diffusivity at a very small water content. The steep slope in the water content profile which includes the inflexion point is often called as drying front (Hillel[3]).

4) *Temperature profile*

The time-change of the temperature profile for $U=150$ cm/s is shown in **Fig. 4**. The following can be inferred from this figure, and a similar figure for $U=290$ cm/s. The temperature at first decreases rapidly before it reaches a minimum value, except in the lower part of the sand layer. Subsequently, it tends to increase toward the initial value. Much of the increase is seen in the upper part of the sand layer for the time, $t=150$–300 h, when the evaporation rate changes exponentially with time, as was shown in **Fig. 1**. The degree of the decrease in the early stages becomes large with decreasing depth, as well as with increasing wind speed. The depth from the sand surface of the minimum temperature value, indicated by z_e, becomes large with time (**Fig. 5**). The temperature gradients, dT/dz, for $z<z_e$ and for $z>z_e$ have opposite signs, where z is the vertical ordinate taken positively downwards, with its origin at the sand surface. Based on heat balance, conductive heat flows toward the location of z_e from both sides must be changed into latent heat for vaporization of liquid water, so that the location of the minimum value is an available index to indicate the place at which evaporation mainly occurs. Let us denote that location "the evaporating front".

Fig. 5 shows the time course of the evaporating front depth, where the closed and open circles are for $U=290$ cm/s and $U=150$ cm/s, respectively. In this figure we observe the following. The evaporating front rapidly moves downwards in the

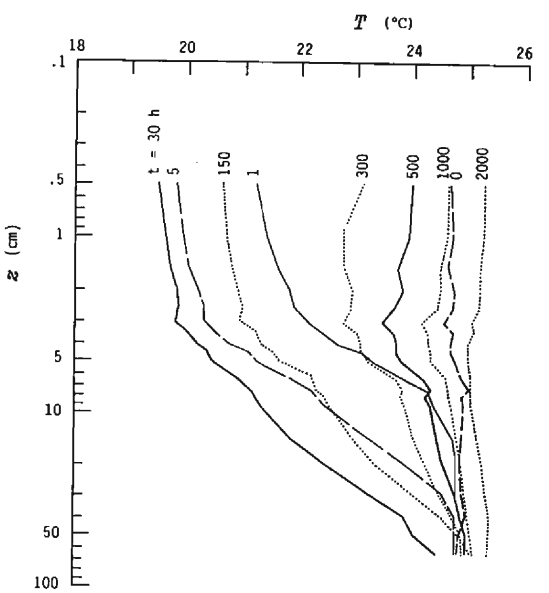

Fig. 4. Changes of the temperature profile with time for Sand K-5 and $U=150$ cm/s.

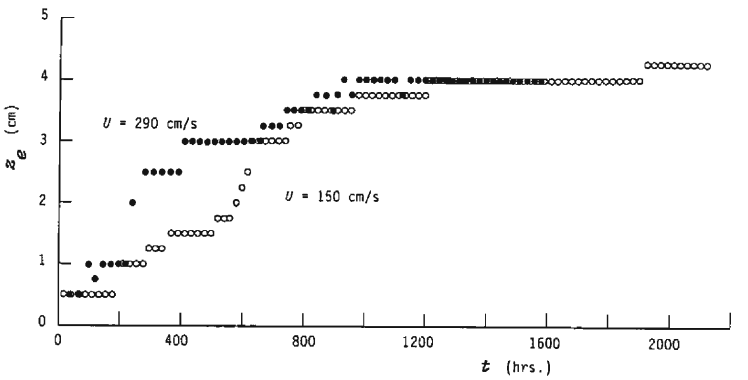

Fig. 5. Advancement of the evaporating front in the case of Sand K-5.

relatively early stages, then its movement decreases with time. Experimental results indicated a depth of 4.5 cm for $U=290$ cm/s ($t=2200$ h), and of 4 cm for $U=150$ cm/s ($t=1600$ h). Thus, the effect of wind speed on the advancement of the evaporating front decreases with time. The results indicate that the front may not stop its downward movement. Concerning the situation in the early stages, the following must be kept in mind. In **Fig. 5** the observed evaporating front seems to move downwards immediately at the outset of the experiment, but since the exposed sand surface at that time is moist enough, the evaporation must occur at the surface for a while. The apparent movement of the evaporating front around at $t=0$ is caused by the difficulty of measuring the temperature at points too close to the sand surface. Although the temperature at 0.5 cm depth was measured, the sand surface temperature was not measured. In comparing **Fig. 1** with **Fig. 5**, the rapid advancement of the evaporating front seems to start in stage-2 when the evaporation rate exponentially decreases with time. The rate of movement in stage-2 becomes larger as the wind becomes strong, but in time (i.e. stage-3), the effect of wind speed on the advancing depth becomes small, as has been noted above. Furthermore, from **Fig. 3** and **Fig. 5**, we can recognize that the evaporating front is located at a depth where a steep slope of the water content profile separates from the BDSR-curve as stated above 3).

(2) The case of Sand K-6

Fig. 6 shows time-courses for the cumulative evaporation, I, for Sand K-6 at several wind speeds at the relatively early stage of the experiment. The time changes in evaporation rate and water table depth at $U=285$ cm/s is shown in **Fig. 7**. From these figures, the following can be recognized. The rapid decrease in the evaporation rate at the outset of the experiment appears to resemble the case of Sand K-5 until the evaporation rate becomes more or less constant (E_1) indicated by the broken lines in **Fig. 6**. Such a constant rate stage was not detected clearly for Sand K-5 which had a particle-size larger than that of Sand K-6. The constant-rate stage ceased at a time ($t=t_1$) accompanied by the occurrence of a sudden drop toward a very small value.

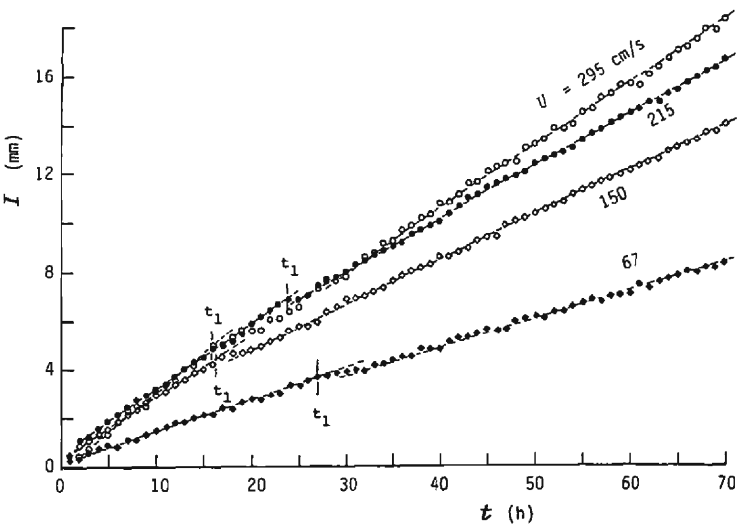

Fig. 6. Changes in the cumulative evaporation with time at a relatively early stage in the case of Sand K-6.

The time, $t=t_1$ decreases with increasing wind speed. In addition, the water table at $t=t_1$ was observed to be in the range of $z_w=25$–29 cm, which was about twice as large as the absolute value of the air entry value, 12 cmH_2O. After the low evaporation rate persisting for a short interval, the rate reaches a constant value (E_2), and a constant-rate stage reoccurs for a while. For example, $E_1=3.01\times10^{-1}$ mm/h and $E_2=2.52\times10^{-1}$ mm/h for $U=295$ cm/s; $E_1=1.28\times10^{-1}$ mm/h and $E_2=1.11\times10^{-1}$ mm/h for $U=67$ cm/s. Subsequently, the evaporation rate seems to decrease exponentially with time (stage-2), e.g., in the interval $t=175$–450 h for $U=285$ cm/s, and the change becomes a very slow decrease with time, as for Sand K-5 (stage-3). The period until the evaporation rate commences to decrease exponentially with time may be considered to be physically equivalent to the stage-1 for Sand K-5. Values of the evaporation rate at stage-1 in the cases of Sand K-6 and Sand K-5, are roughly equal

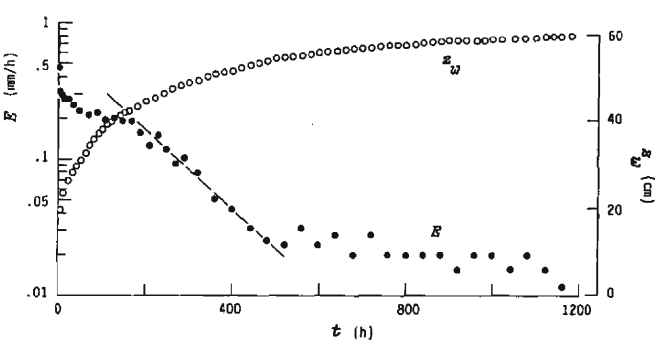

Fig. 7. Changes in the evaporation rate and the water table depth with time for Sand K-6 and $U=$ 285 cm/s.

each other for the same wind speed. It has been shown that the time course of evaporation rate for Sand K-6 is fairly similar to that for Sand K-5, but the change for sand K-6 (finer sand) is, on the average, slower than that for Sand K-5 (coarser sand). Additionally, the relationship wherein the cumulative evaporation becomes larger with increasing wind speed, is satisfied as in the case of Sand K-5.

From **Fig. 7** (also **Fig. 17**) and **Fig. 2**, the water tables for Sand K-6 and Sand K-5 are shown to fall with time in a similar manner, with the case of Sand K-6 is being more pronounced and rapid. We can also see the relationship between the rate of fall and wind velocity as with Sand K-5.

When the evaporation rate showed an unusual change, i.e. a temporary drop as described above, it was observed that the temperature near the sand layer temporarily increased slightly. The correspondence between the two changes follows the law of heat balance. This unusual change of evaporation rate has been observed in a column experiment using a sandy soil by Nakano (1977)[8].

(3) The case of Akadama-soil

1) *Evaporation rate*

Change in the evaporation rate on a logarithmic scale against time at $U=$ 290 cm/s for Akadama-soil is shown by the open circles in **Fig. 8.** In this figure, it seems that the evaporation rate continues to decrease with time up to the end of experiment, $t=750$ h, following a straight line, except at a stage just at the outset of the experiment. This characteristic change is similar to that in stage-2 which was observed in the sand layers. The exponential decay coefficient for the evaporation rate is smaller than that for the sand (see **Table 2**).

2) *Water table depth*

The time-change in the water table depth differentiated with respect to time, dz_w/dt, on a logarithmic scale is also shown in **Fig. 7**, using closed circles. In this figure, the observed data seem to decrease following a straight line except at the outset of the experiment, so that we may conclude that the water table depth increases exponentially

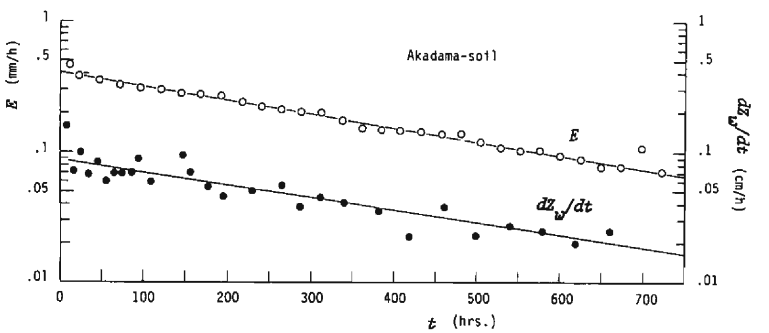

Fig. 8. Time courses of the evaporation rate and the water table depth differentiated with respect to time in the case of Akadama-soil.

with time (also see **Table 2**).

3) *Wetness and temperature near the soil surface*

When the porous massive particles of Akadama-soil were wet or dry, they clearly appeared either brown or whitish-red in colour, respectively. The colour of the surface of the porous material layer changed from brown to whitish-red with time, but the change was not spatially uniform as in the case of the sand. The part that dried out first was the upper surface of the particles located at the top of the layer, and seemed to have less contact with other particles. The drying part extended to the entire area of the exposed surface with time. The whitish-red part did not penetrate deeply, and seemed to stay near the surface of the layer. Furthermore, in this case the surface temperature was measured, and the point of a minimum temperature in the layer, at most times remained at 0.5 cm depth. In addition, at the end of experiment (t= 750 h), the water table reached 30 cm depth (ref. **Fig. 15**). The point of minimum temperature in the soil layer was roughly consistent with the depth of the boundary between brown and whitish-red parts. Therefore, we may conclude that the evaporation occurred at a fixed depth close to the surface, unlike the case of the sand.

(4) The case of glass beads

1) *Evaporation rate*

The time-courses of the evaporation rate for Bead-1, with the biggest particle-diameter and for Bead-3, with the smallest diameter, are shown in **Figs. 9**(**a**) and (**b**), respectively, where closed and open circles represent U=290 cm/s and U=150 cm/s, respectively. From these figures and a similar figure for Bead-2, the following can be shown. The evaporation rate at the stronger wind speed is always larger than that for the weaker one, in the cases of Bead-1 and Bead-2. This relation is of course satisfied within the limitation of this experiment. In the case of Bead-3, this relation is also satisfied at a relatively early stage, but as t increases, the effect due to the magnitude of wind velocity becomes unclear. The results indicate that there is no instance in which the evaporation rate under stronger wind becomes smaller than one for weaker wind from a time in the course of the experiment, as in the case of sand layer. In the

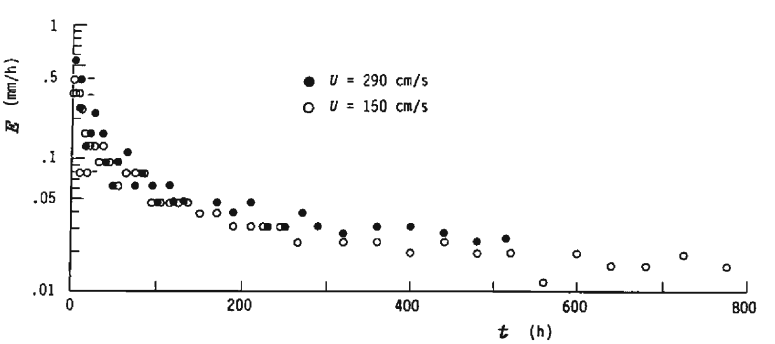

(a) in the case of Bead-1.

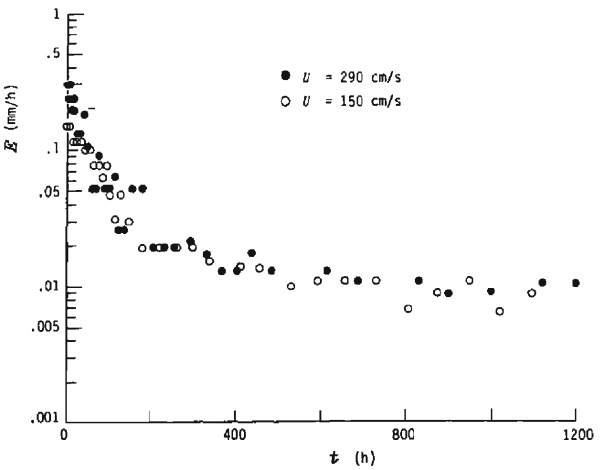

(b) in the case of Bead-3.

Fig. 9. Changes in the evaporation rate with time.

cases of Bead-1 and Bead-2, the stages when the evaporation rate becomes more or less constant (stage-1), and the rate decreases exponentially with time (stage-2), which were detected for the sand layer, seemed not to appear. In the case of Bead-3, the exponential decay did seem to appear at t=25–100 h for U=290 cm/s and t=50–140 h for U=150 cm/s.

Fig. 10 shows changes in the cumulative evaporation rate (I) with time for all glass bead layers, where circles, squares and triangles correspond to Bead-1, Bead-2 and Bead-3, respectively, and closed and open symbols represent U=290 cm/s and U=150 cm/s, respectively. When the wind velocity is fixed at 290 cm/s or

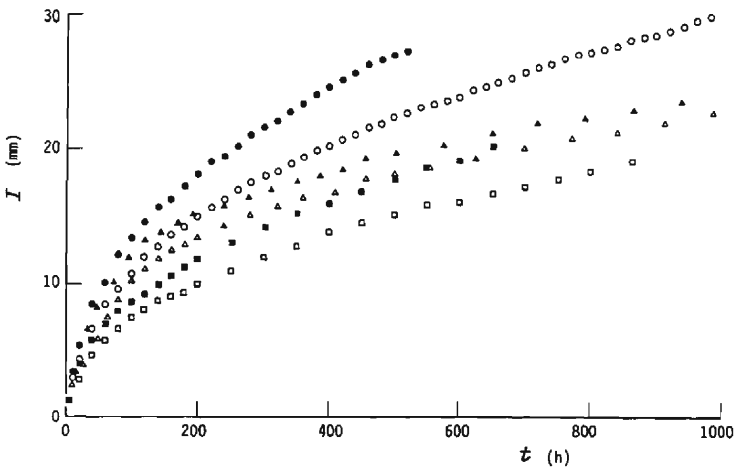

Fig. 10. Changes in the cumulative evaporation with time in the case of glass bead layers.

150 cm/s, the cumulative evaporation at a point in time becomes larger in the order of Bead-1, Bead-3, and Bead-2, within the range of our data. This result is of interest, because this order is not consistent with the order of the particle-sizes. However, at $U=290$ cm/s, and $t=700$ h and later, the order is supposed to change to Bead-1, Bead-2, Bead-3 in accordance with the order of particle sizes.

2) *Water table depth*

Time courses of the water table depth for Bead-1, Bead-2 and Bead-3 are shown in **Figs. 19(a)** to **(c)**, where closed and open circles represent $U=290$ cm/s and $U=150$ cm/s, respectively. The time-axis for the case of $U=150$ cm/s is multiplied by the ratio (<1) of both friction velocities, as stated in Chapter 4, except in the case of Bead-1. The time axis at $U=150$ cm/s for Bead-1 is multiplied by a factor ($=0.58\approx 1/1.75$). The following may be concluded from these figures. The water table at first falls relatively rapidly, and then the subsiding as in the case of the sand layer. **Fig. 10** indicates that the decrease is faster as the wind becomes strong. It was shown that the rate of decrease was not necessarily in the order of particle-sizes, as the order proved to be in the order of Bead-3, Bead-1 and Bead-2. The water table is defined by the point where the water pressure is zero, and the capillary rise was larger in the order of Bead-3, Bead-2 and Bead-1, so that the order for the degree of fall of the water table does not necessarily correspond to the one for the cumulative evaporation stated above. Compared with the time change in the water table depth for the sand layer, the fall of water table is very small in this case, as for example, the depth for Bead-3 at $U=290$ cm/s increased to only about 12 cm even after three and a half months (see **Fig. 11**), and that for Bead-1 at $U=150$ cm/s reached 8 cm after one and a half months.

3) *Evaporating front depth*

Fig. 11 shows the advancement of the evaporating front indicated by the minimum temperature in the Bead-3 layer at $U=290$ cm/s, using closed circles. Open circles represent the water table depth. From **Fig. 11** and, the similar graphs for Bead-1 and Bead-2, the following was concluded. In the cases of Bead-1 and Bead-2, the

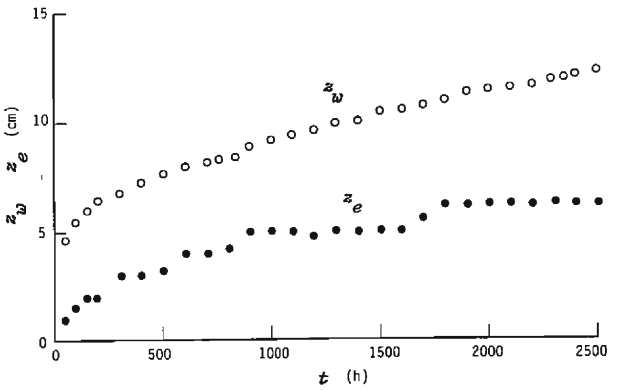

Fig. 11. Changes in the evaporating front and water table depths with time in the case of Bead-3 at $U=290$ cm/s.

difference between water table depth (z_w) and evaporating front depth (z_e) is constant, except when the water table falls to a shallow depth, and the value of (z_w–z_e) approaches zero for Bead-1, and 1 cm for Bead-2. These values are fairly consistent with the capillary rise in height. This indicates that as the pore size of the layers increases, the liquid water movement upward from the upper edge of the saturated zone, hardly occurred, and the evaporation had to occur at this edge. In the case of Bead-3, the value of (z_w–z_e) was about 4 cm until around 1500 h, and after this time seems to increase although not greatly. The same characteristic as (z_w–z_e), was also detected at U=150 cm/s. The value of 4 cm seems to be larger than that of capillary rise, so that the evaporation situation for Bead-3 may be said to lie between that for Bead-1 and Bead-2 layers, and the sand layers.

4. Analysis and Discussion

4.1 Fundamental Equations

(1) Below the surface of the porous material layer

Let us focus on the situation in which evaporation occurs below the exposed surface of porous material layer. When the evaporating zone is approximated as a horizontal plane located at $z=z_e$, we may analyse the movement of water, by separating the material layer into two regions (Barnes & Allison (1983[9]), 1984[10]), Allison et al (1983)[11]), Ishihara et al (1989)[12]), Shimojima et al (1989)[13]). One is the region below the evaporating front, $z>z_e$, and the other is the region above that front, $0<z<z_e$. Water in both regions may be dealt with in their liquid and gas phases, respectively. We respectively denote the regions, "L-region" and "V-region" (see Section 2(1)). In the following analysis, we consider such a plane to be the evaporating zone.

1) *Liquid water*

The movement of liquid water in a porous material layer such as the sand obeys Darcy's law given by the next equation.

$$V_l=-K\{1-\partial p_w/\partial z\} \tag{1}$$

or

$$V_l=-K+D\partial\theta/\partial z, \tag{2}$$

where V_l is the filter (Darcy) velocity of the water, K the hydraulic conductivity, p_w the water pressure (matrix potential) in the water head and D the moisture diffusivity defined by:

$$D=Kdp_w/d\theta \tag{3}$$

In Eq. (2) we have neglected the effect of the temperature gradient as a driving force for the liquid movement (Philip & De Vries (1957)[14]). In addition, as has been already defined, z is an ordinate taken positive downward, and its origin is set at the surface of porous material layer.

The continuity equation for the water is given by:

$$\partial\theta/\partial t+\partial V_l/\partial z=-e, \tag{4}$$

where e is the strength of evaporation at z and can be put at zero in the L-region.

The water content profile is formally given by integrating Eq. (2) as:

$$z=z_w-\int_{\theta}^{\theta_{sat}} D/(V_l+K)d\theta. \tag{5}$$

2) *Water vapour*

Water vapour caused by the evaporation at $z=z_e$ is carried up to the exposed surface of porous material layer through the V-region. The driving force is mainly based on a diffusion effect, so that the transfer equation is given by:

$$\rho_v V_v=-D_s^{eff}\partial\rho_v/\partial z, \tag{6}$$

where ρ_v is the density of water vapour, V_v the filter velocity of water vapour, and D_s^{eff} the effective diffusivity for water vapour in the porous material layer.

In particular, when the mass flux of the water vapour, $(\rho_v V_v)$, in the V-region can be considered to be quasi-steady, Eq. (6) is rewritten as:

$$\rho_w E=D_s^{eff}\partial\rho_v/\partial z, \tag{7}$$

where ρ_w is the water density, and E the evaporation rate (>0), as defined previously and which has a dimension of [Length/Time].

D_s^{eff} has been considered to be based only on effective molecular diffusion D_{sm}^{eff} (Philip & De Vries[14]). However, by recognizing the effect of the turbulent wind above the surface of the porous material layer on the water vapour transfer in the V-region (Farrell et al (1966)[15], Scotter & Raats (1969)[16], Ishihara et al (1988)[17]), we assume here that D_s^{eff} is represented by the sum of D_{sm}^{eff} and the effective turbulent diffusivity for water vapour, D_{st}^{eff}. D_{sm}^{eff} and D_{st}^{eff} may be represented by (Barnes & Allison[10] for D_{sm}^{eff}):

$$D_{sm}^{eff}=\tau\theta_a D_{sm} \tag{8}$$

and

$$D_{st}^{eff}=\tau\theta_a D_{st}, \tag{9}$$

where τ is the tortuosity, θ_a the porosity (assumed constant), D_{sm} the coefficient of molecular diffusion of water vapour in still air, and D_{st} the intrinsic turbulent diffusivity of water vapour in pores. A function of D_{st}^{eff} may be considered to be in proportion to u_* at a specified depth as a first approximation, so that D_{st}^{eff} is written as:

$$D_{st}^{eff}=u_* L_s, \tag{10}$$

where L_s is dependent on depth and it must decrease with increasing depth (Ishihara et al[17]). L_s has the dimension of length.

(2) Above the surface of the porous material layer

When the Reynolds analogy between transfers of water vapour and momentum,

in a turbulent boundary layer developing above the surface of a porous material layer is satisfied, the evaporation rate is determined through the next equation (Brutsaert[2]).

$$E=\{u_*^2/U_b\rho_a(q_0-q_b)\}/\rho_w, \tag{11}$$

where u_* is the friction velocity, ρ_a the mass density of air, q the specific humidity and the subscripts, "0" and "b" denote the values at $z=0$ and at $z=z_b$, the outer edge of the boundary layer, respectively, and U_b is the wind velocity at $z=z_b$.

In the following examination, integrating Eq. (6) with respect to z between $z=z_e$ (evaporating front depth) and $z=0$, and eliminating q_0 from the resultant equation and Eq. (11), we obtain the next equation.

$$E=\rho_a/\rho_w(q_e-q_b)\Big/\Big[\int_0^{z_e}\{1/(D_{sm}^{eff}+D_{st}^{eff})\}\,dz+(U_b/u_*^2)\Big] \tag{12}$$

or

$$E/u_*=\rho_a/\rho_w(q_e-q_b)\Big/\Big[\int_0^{z_e}\{1/(D_{sm}^{eff}/u_*+D_{st}^{eff}/u_*)\}\mathrm{d}z+(U_b/u_*)\Big] \tag{13}$$

When D_{st}^{eff} is given by an exponential function as (Ishihara et al[17])

$$D_{st}^{eff}=D_{st0}^{eff}\exp(-z/z_*), \tag{14}$$

where D_{st0}^{eff} is D_{st}^{eff} at $z=0$, z_* (=const.) a characteristic penetration depth of the turbulent effect due to an applied wind, under the condition that $D_{st}^{eff}\ll D_{sm}^{eff}$ at $z=z_e$, Eq. (12) is approximated by:

$$E=A/(B+z_e), \tag{15}$$

where

$$A=(\rho_a/\rho_w)D_{sm}^{eff}(q_e-q_b), \tag{16}$$

and

$$B=-z_*\ln\{(D_{sm}^{eff}+D_{st0}^{eff})/D_{sm}^{eff}\}+D_{sm}^{eff}/(u_*^2/U_b). \tag{17}$$

In the above derivation, water content, $\theta_{sat}-\theta_a$ in the V-region ($0<z<z_e$), has been assumed constant. Eq. (15) gives an important relation between evaporation rate and evaporating front depth.

4.2 Effect of the Wind Speed on the Evaporation

(1) Relationship between the evaporation rate and the water table depth

1) *Theoretical relation*

Referring to the observed water content profiles for Sand K-5 in **Fig. 3**, we obtain the schematic water content profile shown in **Fig. 12**. In this figure, θ_c is a value of θ which is more or less consistent with the field capacity, θ_e a representative value of θ in the evaporating front assumed to be constant, θ_r ($=\theta_{sat}-\theta_a$) the residual value of θ, i.e., an air-dried value after the evaporating front has passed by, z_c the depth at $\theta=\theta_c$, and z_w' the depth of the capillary fringe. The magnitude of z_e is dependent upon the degree of the progress of the evaporation (ref. **Fig. 5**). **Fig. 3** shows the situation after a significant amount of time has elapsed, so that when the evaporation occurs at the surface of the porous material layer, i.e., $z_e=0$, the θ-value at the evapo-

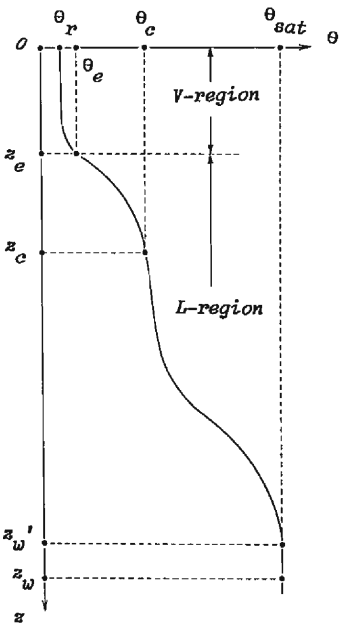

Fig. 12. A schematic water content profile.

rating front is consistent with water content, θ_0, at $z=0$, and the value is within the range where $\theta_e<\theta<\theta_{sat}$. In the case of a glass bead layer such as Bead-1 or Bead-2, based on the evidence stated in Chapter 3 (4), we can set $z_e=z_w'$ and the distance between $z=z_e$ and $z=z_w'$ is negligibly small.

Let us here focus on a specified porous material layer. For simplicity of expression, let us denote the zone in which the turbulent boundary layer develops over the surface of the porous material layer, as the A-region ($0>z>z_b$). Looking at the right side of Eq. (13), D_{st}^{eff}/u_* is known from Eq. (10) to be a function of only z, and U_b/u_* may be assumed to be constant (see; 2)). Under the assumption that the value of $\rho_a(q_e-q_b)$ at a specified value of z_e is uniquely determined regardless of wind speeds, the following can be said. When $D_{st}^{eff}\gg D_{sm}^{eff}$ in the V-region, E/u_* given by Eq. (13) must be constant at a specified evaporating front depth regardless of wind speeds. However, as the evaporating front depth increases, the contribution of molecular diffusion to the water vapour transfer in the V-region becomes much larger in magnitude than that of turbulent diffusion. This indicates that the molecular diffusion term of the integral in the right side of Eq. (13) becomes much larger than the turbulent diffusion one. Therefore, when $D_{st}^{eff}\ll D_{sm}^{eff}$ for $z_e>z>z_p$ in the V-region and $z_e\gg z_p$ where z_p is a depth, E/u_* must depend on wind speed (U) or the friction velocity (u_*) even at a fixed value of z_e. Instead, E becomes independent of u_*, that is, E becomes uniquely determined by the evaporating front depth, z_e. We denote both situations as "W-range" and "S-range", in order.

In the above consideration, we have assumed that the evaporation occurred below the surface of porous material layer. When the evaporation occurs at the

surface, Eq. (11) is not doubt satisfied, but Eqs. (12) and (13) are not applicable. In this case, the water vapour at the surface must be saturated unlike the case where $z_e>0$ and depends on only the surface temperature. When the value of (q_0-q_b) is uniquely determined regardless of wind speed, Eq. (11) leads us to the conclusion that E/u_* is not dependent on wind speeds.

2) *Experimental relation*

a) *Sand*

Relationship between E or E/u_* and z_w:

Figs. 13(a) and **(b)** show the relationship between the logarithm of the evaporation rate and the water table depth at a given time, in the cases of Sand K-5 and Sand K-6, respectively. **Figs. 14(a)** and **(b)** are graphs in which the ordinate represents the evaporation rate of **Figs. 13(a)** and **(b)**, divided by the friction velocity of applied airflow, u_*. The value of u_* was obtained from a wind speed profile in the A-region using a hot-wire anemometer, giving the following results. In the case of Sand K-5, $u_*=19.5$ cm/s at $U=290$ cm/s, and $u_*=10.0$ cm/s at $U=150$ cm/s. In the case of Sand K-6, $u_*=13.6$ cm/s at $U=295$ cm/s; $u_*=13.1$ cm/s at $U=285$ cm/s; $u_*=10.6$ cm/s at $U=215$ cm/s; $u_*=7.9$ cm/s at $U=150$ cm/s; $u_*=5.3$ cm/s at $U=67$ cm/s. In addition, it is known from these values that u_* is more or less proportional to $U(=U_b)$ for each sand layer. **Fig. 13** and **Fig. 14** incorporate the fact that the evaporation rate

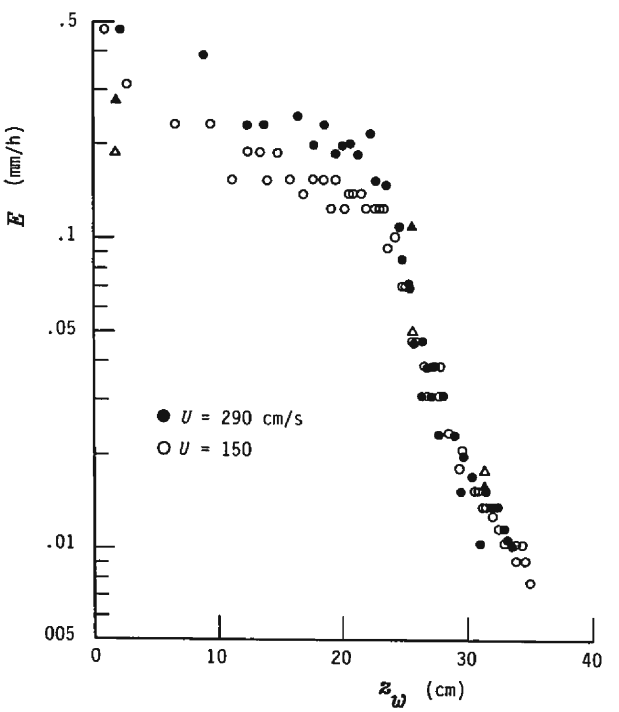

(a) in the case of Sand K-5.

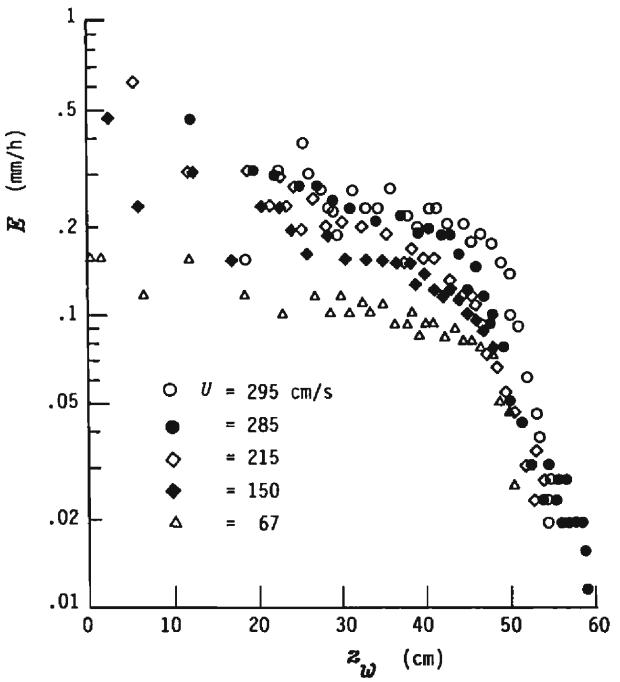

(b) in the case of Sand K-6.

Fig. 13. Relation between E and z_w.

first decreases moderately with increasing water table depth, and then commences to decrease abruptly at the depth, $z_w=z_{wc}$. The value of z_{wc} for each sand layer is more or less constant regardless of applied (mean) wind velocity, and it is roughly 25 cm and 45 cm, for Sand K-5 and Sand K-6, respectively. The values of E/u_* for several wind velocities seem to lie on a curve, beyond the range of $z_w<z_{wc}$ regardless of velocity. As z_w becomes larger, the values of E/u_* for each wind velocity diverges, but E-values for each velocity lie on a curve. These tendencies are qualitatively consistent with the results theoretically inferred in 1).

The surface of sand layer must be moist enough in the range of $z_w<z_{wc}$, so that the water content profile may be represented by the BDSR-curve with good accuracy. In addition, when z_w is smaller in magnitude than the absolute value of the air entry value, $p_w{}^{en}$, the water content at $z=0$ is that at saturation. $p_w{}^{en}$ is -12 cmH_2O for Sand K-6 and -5 cmH_2O for Sand K-5. Volumetric water content, θ_0', obtained by applying the value of $-z_{wc}$ to the BDSR-curve as the matrix potential, is about 0.075 for Sand K-5 and about 0.12 for sand K-6. The field capacity, θ_f is roughly 0.04 for both sand layers. The value of θ_0', 0.075, for Sand K-5 was shown to be relatively close to the value of θ_f. The value, 0.12, for Sand K-6, is more or less consistent with a water content at which the BDSR-curve shows a inflexion point just before approaching the field capacity. Applying the water content, θ_0', when $z_w=z_{wc}$, to Kelvin's relation (Philip & De Vries[14]), it was supposed that the water vapour

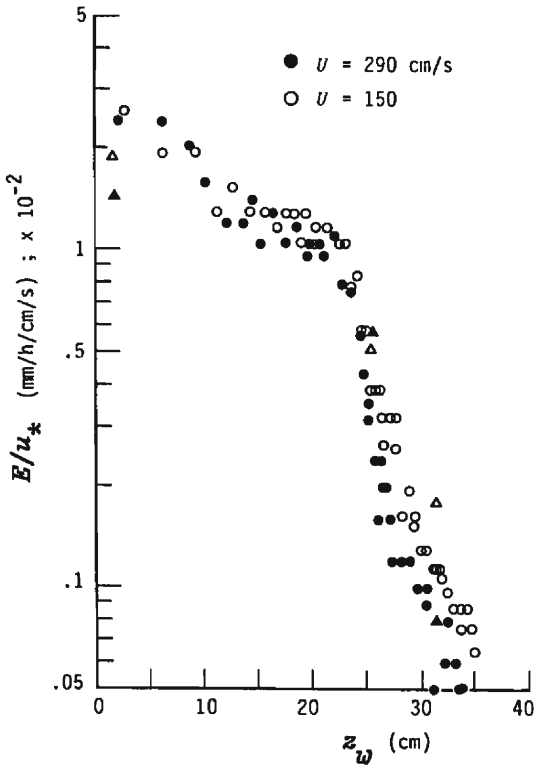

(a) in the case of Sand K-5.

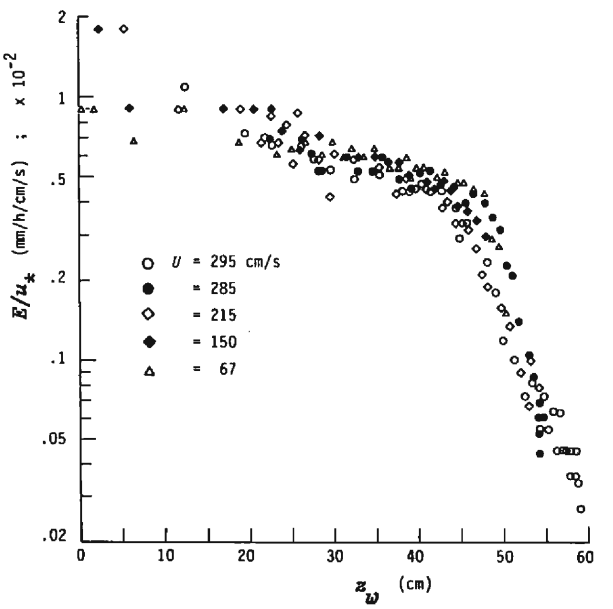

(b) in the case of Sand K-6.

Fig. 14. Relation between E/u_* and z_w.

at the surface was practically saturated at least for $z_w<z_{wc}$. In fact, for example, in **Fig. 5** when z_w increased to roughly z_{wc}, the evaporating front seemed to start to move downward rapidly (in stage-2). Thus, we can conclude that the evaporation for $z_w<z_{wc}$ occurred at the sand surface (ref. Kuzuha et al[6]).

As stated in Chapter 3, the following was observed in the case of the sand layer. The temperature near the sand surface at an early stage of the experiment decreases markedly with time, and the decrease becomes more pronounced with the increase of U, i.e., u_*. For example, in the case of Sand K-5, it was recognized that the discrepancy between time courses in the temperature at 0.5 cm depth, i.e. closest to the sand surface for $U=290$ cm/s and for $U=150$ cm/s was within 1.5°C at the same water table depth. This indicates that (q_0-q_b) in the both cases showed more or less the same value at a fixed value of z_w regardless of wind velocity. In fact, we can understand, through Eq. (11), why the experimental data of E/u_*, at least in the range $z_w<z_{wc}$, are dependent on only z_w, regardless of the wind velocity.

Characteristics of liquid flow just below the evaporating front:

The triangles in **Fig. 13(a)** and **Fig. 14(a)** indicate a relationship between E or E/u_* and z_w obtained at steady state in an experiment under the condition of a water table of fixed depth. The experiment was run using the same Sand K-5 layer as heretofore with an initial water content profile consistent with the BDSR-curve (Ishihara et al (1989)[12]). Closed and open triangles correspond to $U=290$ cm/s and $U=150$ cm/s, respectively. In these figures, values of E or E/u_* for the restricted water table seem to be consistent with the unrestricted condition, except when the water table was set at 1.3 cm depth. The evaporating front depth (z_e) for the restricted water table was found to be, for example, about 1 cm for $z_w=25.5$ cm and about 3 cm for $z_w=31.3$ cm regardless of wind velocity. From **Fig. 2** and **Fig. 5**, the values of z_e for the unrestricted water table when $z_w=25.5$ cm $(=z_{wc})$ and 31.3 cm $(>z_{wc})$, were found to be nearly equal to the values for the restricted condition regardless of velocity. This indicates that the evaporating front depth is mainly determined by water table depth, regardless of wind velocity, though this relation is obviously not satisfied when the evaporation occurs at the sand surface as in the case of $z_w=1.3$ cm. The inconsistency of E or E/u_* for $z_w=1.3$ cm in both water table conditions can be explained by consideration of the density of saturated water vapour at the sand surface, caused by the difference in the temperature fall at the surface, but this detail is not considered here to avoid redundancy.

We write the evaporation rate (E) for the unrestricted and restricted water tables as $E^{(ur)}$, and $E^{(r)}$, respectively. In Eq. (1), the relation that $-V_l \ll K$ may be satisfied for $\theta_{sat}>\theta>\theta'$, so that Eq. (5) at $z=z_e$ is approximated by

$$z_e=z_w-\int_{\theta'}^{\theta_{sat}} D/K\mathrm{d}\theta-\int_{\theta_e}^{\theta'} D/(V_l+K)\mathrm{d}\theta, \tag{18}$$

where θ' is a constant, and is larger than θ_e.

The liquid flow rate, V_l, in the sand layer for the restricted water table is constant with respect to time and depth, while for the unrestricted water table, the flow condition

is not necessarily satisfied throughout an entire domain because, for example, $V_l=0$ at $z=z_w$. This result indicates that whether water table is unrestricted or restricted does not have a great effect on the evaporation rate, but rather that the magnitude of water table depth directly affects the evaporation rate. Applying these results to Eq. (18), the third term on the right side must be the same at a specified water table depth regardless of either the restricted or unrestricted water table condition, because z_e is uniquely determined by giving a value to z_w. By taking account of the functional property of K which will be set forth in Section 3 (Eq. (22)), K for $\theta_e<\theta<\theta'$ may be negligibly smaller in magnitude than E $(=E^{(r)})$ for the restricted water table, so the third term becomes R $(\theta_e, \theta')/E^{(r)}$, where R is an integral of D with respect to θ from $\theta=\theta_e$ to $\theta=\theta'$. On the other hand, in the case of the unrestricted water table, the third term must be consistent with $R/E^{(r)}$ as stated just above, so that V_l in the region where $\theta_e<\theta<\theta'$ is consistent with $-E^{(ur)}$ in magnitude. This indicates that in the flux-concentration relation (Philip (1973)[18]), $-V_l/E^{(ur)}$, in the region where $\theta_e<\theta<\theta'$ must increase to unity from zero at $z=z_w$ with decreasing depth. This condition of liquid water flux, in which $-V_l/E^{(ur)}$ approaches unity, can be varified in a different fashion, e.g., through an analysis of isotopic behaviour in a sand column (Shimojima et al[13]).

b) *Akadama-soil*

The only wind velocity applied to Akadama-soil was $U=290$ cm/s. When we plot the evaporation rate against water table depth using circles, we obtain **Fig. 15.** From this figure the following is observed. The evaporation rate continuously decreases with the increasing depth of the water table for the duration of the trial, following the broken straight line in the figure, where the line is represented by the function E (mm/h) $=0.0107\ z_w$ (cm) $+0.405$. This characteristic change was not observed over the entire extent of the experiment, as in the case of the sand layer. Though the data are plotted on a normal graph, unlike **Fig. 13**, there seems to be no characteristic water table depth like the z_{wc} detected for the sand layer. The rapid decrease in the evaporation rate with the increasing water table depth, as seen in the case of the sand, in the range $z_w>z_{wc}$, does not occur in this case. This fact is strongly related to experimental evidence that the evaporation continued to occur close to the surface of the layer, because the appearance of an abrupt decrease in the evaporation rate

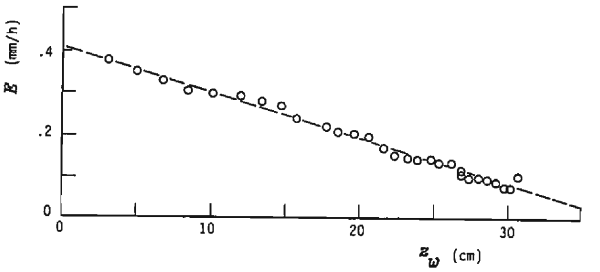

Fig. 15. Same as Fig. 13. but for the case of Akadama-soil.

with the water table depth for the sand layer roughly corresponded to the remarkable advancement of the evaporating front as stated in a).

c) *Glass bead*

Fig. 16(a) shows the relationship between the evaporation rate and the water table depth observed in the case of the biggest glass bead, Bead-1. In this figure only the value of evaporation rate at $U=150$ cm/s is multiplied by a factor, $1/\beta$ ($=1.75$), in order to obtain a good agreement with the data at $U=290$ cm/s. The estimation of u_* from wind velocity profile observed in the A-region was complicated by irregularity in the surface of the glass bead layer unlike the smooth surface of the sand layer. The irregularities in the surface of the glass bead layer had a comparable order in magnitude as the thickness of the turbulent boundary layer, approximately 1 cm. However, values of 30 cm/s and 10 cm/s, at $U=290$ cm/s and $U=150$ cm/s, respectively, were obtained as the approximate values of u_*. The ratio of these values of u_* is about 3, which is not close to that of $1/\beta$ ($=1.75$). Based on the result for the sand layer, discussed in a), this disagreement must be caused by a poor estimation of the value of u_*. Nevertheless, **Fig. 16(a)** shows that the function of the evaporation rate with respect to the water table depth is uniquely determined over the entire extent of the experiment by introducing the scaling factor β to the evaporation rate at any wind velocity. As stated in Chapter 3, in the case of Bead-1, we can consider the water table as the evaporating front. Even after the water table has dropped to about 4 cm depth which corresponds to 3–4 bead particles, there exists a clear and significant difference between both of the evaporation rates, so that we may state that the wind continuously affects the evaporation rate through the friction velocity.

Figs. 16(b) and **(c)** are similar to **Fig. 16(a)**, but correspond to Bead-2 and Bead-3, respectively, and the ordinates represent the evaporation rate divided by the friction velocity, for each applied wind velocity. The value of u_* in the case of Bead-2

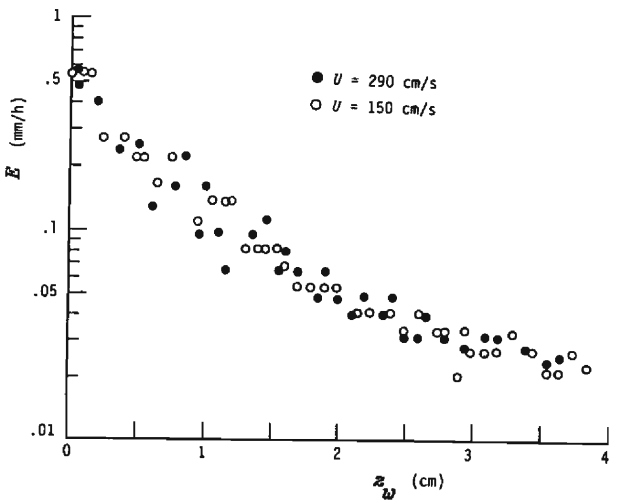

(a) in the case of Bead-1.

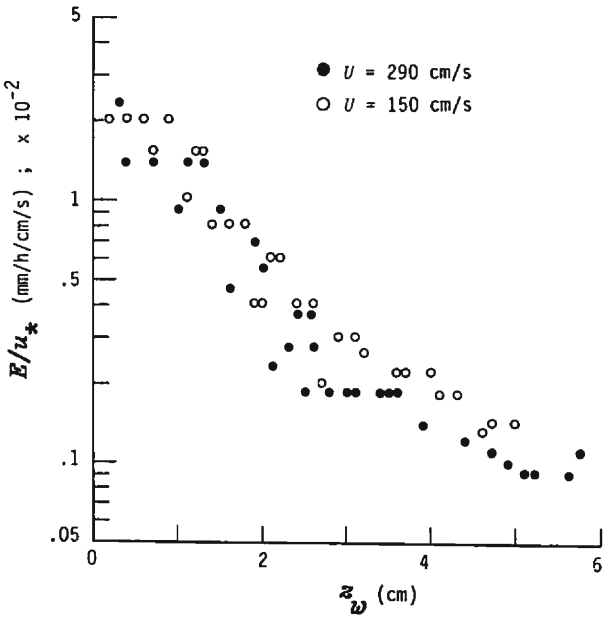

(b) in the case of Bead-2.

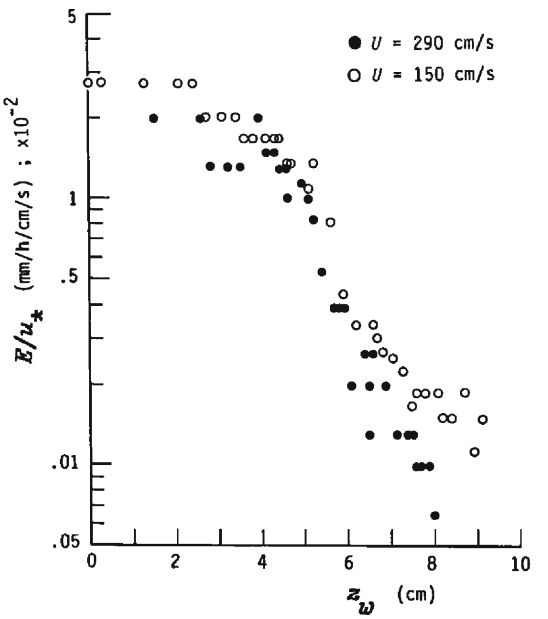

(c) in the case of Bead-3.

Fig. 16. Relation between the evaporation rate and the water table depth.

is 16.7 cm/s at $U=290$ cm/s and 7.6 cm/s at $U=150$ cm/s, and, in the case of Bead-3, $u_*=11.8$ cm/s at $U=290$ cm/s and $u_*=5.7$ cm/s at $U=150$ cm/s. u_* is fairly proportional to U in magnitude. From these figures the following is understood. The value of z_{wc} is about 1 cm for Bead-2 and 4 cm for Bead-3. The value of 1 cm for Bead-2 is fairly consistent with the capillary rise in height ($=-p_{w^{en}}$), so that water content at the surface, when z_w has increased to z_{wc}, is in a transitional state between saturation and unsaturation. The value of 4 cm for Bead-3 appears to be larger than the absolute value of $p_{w^{en}}$, but it is consistent with the distance between the evaporating front and the water table, a condition which was satisfied before significant time had elapsed, as stated in Chapter 3 (4) 3). The values of E/u_* for fixed values of z_w in the case of Bead-2, are uniquely determined over the entire experiment regardless of wind velocity. However, in the case of Bead-3, the same relation is satisfied up to about 6 cm of water table depth, but as the depth increases, the data for two wind speeds diverge. After the divergence for both cases in the relation between E/u_* and z_w had appeared, we understood that the relationship between E and z_w was uniquely determined regardless of wind velocity, as in the cases of the sands.

In conclusion, in the cases of Bead-1 and Bead-2 with large pore-diameter (on the order of 10 mm), the turbulent wind continued to markedly affect the water vapour transfer in the V-region, and the W-range persisted to the end of experiment. On the other hand, in the case of Bead-3 with relatively small pore-size (on the order of 1 mm), that effect was smaller in magnitude, as it was for the sand layer, and the S-range following the W-range appeared with increasing water table depth.

(2) Relationship between the moving velocity of the water table and the wind velocity

1) *Theoretical relation*

Let us focus on the W-range in which the water vapour transfer in the porous material layers occurs mainly by means of turbulent diffusion, even when evaporation occurs below the surface of the layer. We have found that the surface of the sand layer in this range maintains a degree of moisture while for the glass bead layer, it is either saturated or dry. For the sand case, the evaporation was expected to have occurred at the surface or close to the surface, so that the water content profile in the sand layer could be approximately represented by the BDSR-curve, as stated before, although the approximation near the sand surface is not necessarily reasonable.

After taking θ and t as independent variables in Eq. (4), where e is set at zero, integrating the resultant equation with respect to θ from $\theta=\theta^*$ to $\theta=\theta_{sat}$, we obtain the next continuity equation.

$$E=\int_{\theta^*}^{\theta_{sat}}\partial z/\partial t\,\mathrm{d}\theta=\int_{\theta^*}^{\theta'}\partial z/\partial t\,\mathrm{d}\theta+(\theta_{sat}-\theta')\mathrm{d}z_w/\mathrm{d}t, \tag{19}$$

where when $z_e=0$, θ^* is θ at $z=0(\theta_0)$ and when $z_e>0$,θ^* is θ_r. In Eq. (19) we made use of the fact that the water content profile for $\theta'<\theta<\theta_{sat}$ is unchangeable as it is represented by the BDSR-curve.

As $dz_w/dt > \partial z/\partial t$ for $\theta' > \theta > \theta^*$ and $(\theta_{sat}-\theta') \gg (\theta'-\theta^*)$, the first term on the right side of Eq. (19) is negligibly smaller than the second term. Then, Eq. (19) can be approximated by:

$$E=(\theta_{sat}-\theta')dz_w/dt \tag{20}$$

Dividing both sides of Eq. (20) by the friction velocity, u_*, yields

$$E/u_*=(\theta_{sat}-\theta')dz_w/d(u_*t). \tag{21}$$

We have experimentally seen that E/u_* in the W-range is a function of only z_w. And $(\theta_{sat}-\theta')$ is a constant. Therefore, Eq. (21) leads us to the fact that z_w is represented by a function of only u_*t.

2) *Examination of the experimental data*

a) *Sand*

Let us examine the experimental data by using Eq. (21). **Fig. 17(a)** shows the time course of the change in water table depth in the case of Sand K-5 at $U=290$ cm/s and $U=150$ cm/s, where the data (closed circles) for $U=290$ cm/s are taken as the standard, and the elapsed time at $U=150$ cm/s (open circles) is divided by a factor, $\alpha=1.6$ (see **Fig. 18**), to obtain good agreement with the standard data particularly in the early stages. In this figure, it seems that the data for both cases agree well until the water table falls to roughly z_{wc} (=25 cm). We denote this factor as the scaling factor of time. **Fig. 17(b)** is the same as **Fig. 17(a)**, but shows the cases of Sand K-6 at $U=285$ cm/s and 215 cm/s, where the data (closed circles) at greater wind velocity, $U=285$ cm/s, are also taken as the standard and the elapsed time of the data (open circles) at $U=215$ cm/s are also modified. We can see from this figure that the data for both cases are in agreement beyond the water table depth of $z_{wc}=45$ cm. At the other wind velocity conditions in the case of Sand K-6, we obtained the same result as in **Fig. 17(b)**. **Fig. 18** shows the relation between the scaling factor of time, α and the inverse of the ratio of the corresponding friction velocities, $1/\beta$, where open and closed

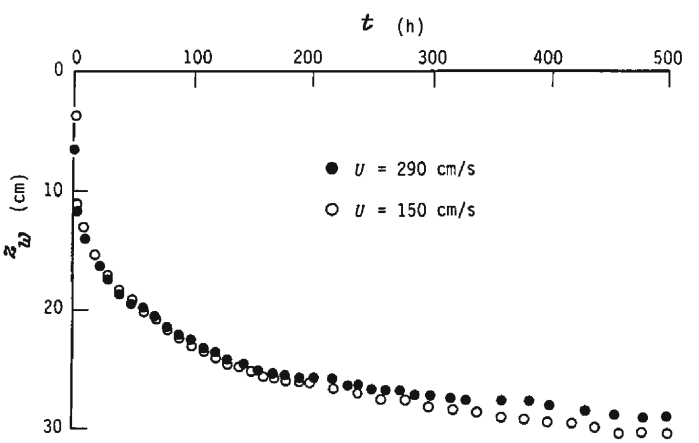

(a) in the case of Sand K-5 ($U=290$, 150 cm/s).

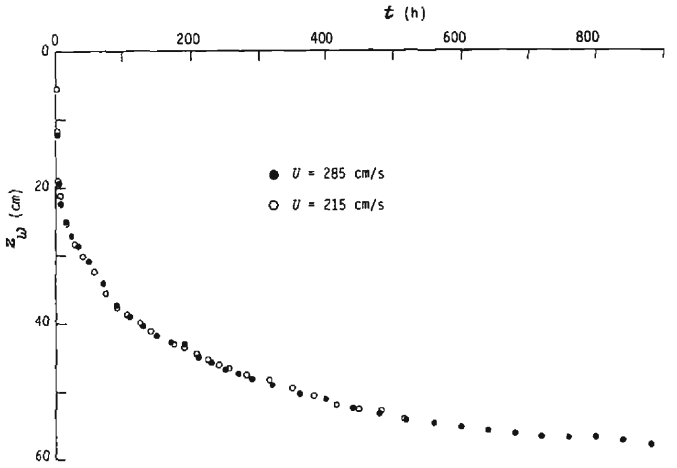

(b) in the case of Sand K-6 (U=285, 215 cm/s).

Fig. 17. Comparison between the time courses of water table depth due to different wind speeds.

circles represent Sand K-5 and Sand K-6, respectively. From this figure, the following can be inferred. The equation $\alpha=1/\beta$ is satisfied, so that $z_w(t)$ at several wind velocities can be similarly scaled with respect to time, using a ratio of the friction velocities until the water table falls to a certain depth. That depth is nearly equal to or greater than that of z_{wc}, as stated above.

b) *Glass bead*

In the cases of Bead-1, Bead-2 and Bead-3, we respectively obtain **Figs. 19(a)** to **(c)**, where the time-axis is taken at U=290 cm/s as the standard, and the time at U=150 cm/s is multiplied by the ratio of the friction velocities (<1), except in the case of Bead-1. In the case of Bead-1, the time is multiplied by 0.58 ($1/\alpha$-value), which is the value of β, 1/1.75, for the evaporation rate obtained in **Fig. 16(a)**. The following can be inferred from these figures. The closed and open circles, representing

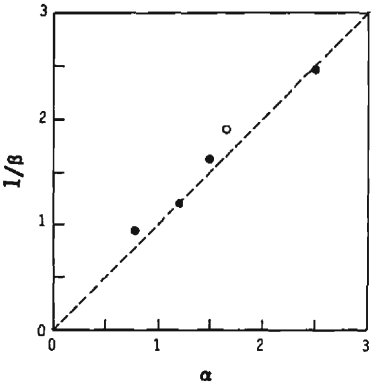

Fig. 18. Relation between $1/\beta$ and α.

Bead-1 and Bead-2, respectively, are in agreement with each other. In the case of Bead-3, agreement is seen until the 6 cm depth of the water table, beyond which disagreement occurs. These results indicate that the W-range is not exceeded in the experiments for Bead-1 and Bead-2, but that a shift from the W-range to the S-range occurs approximately at $z_w=6$ cm for Bead-3. These existing situation of the ranges against water table depth assure the same results obtained in **Fig. 16**, but from a different point of view.

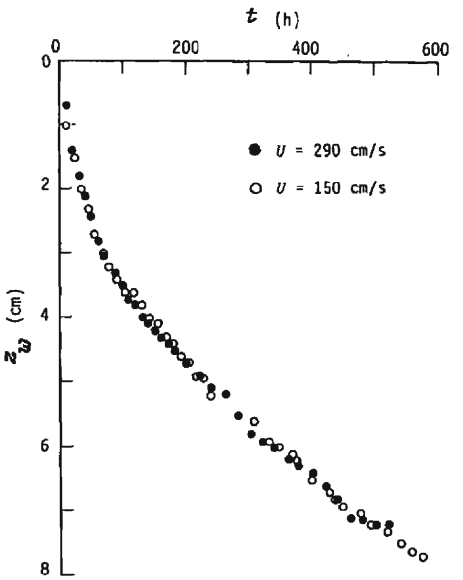

(a) for Bead-1.

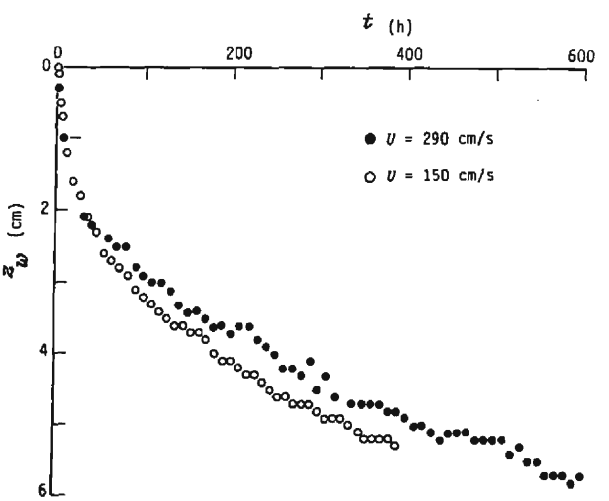

(b) for Bead-2.

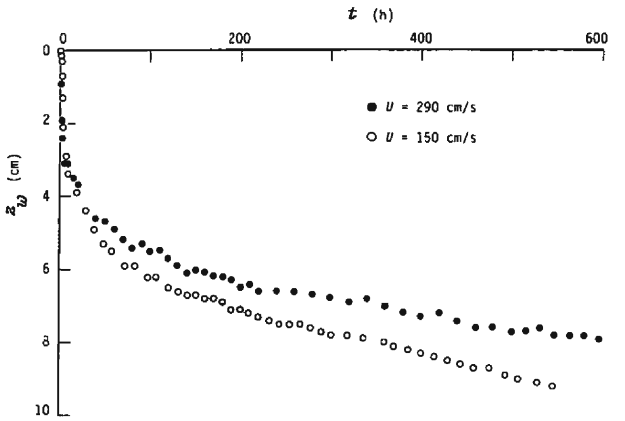

(c) for Bead-3.

Fig. 19. Same as Fig. 17. but for the case of glass bead layers.

4.3 Time Courses of the Evaporation Rate and the Water Table Depth

In this section we examine the time courses of evaporation rate and water table depth, focusing on two specific stages. One of them is the stage in which an exponential decay of evaporation rate occurs in the sand and Akadama-soil layers. The other is the stage following a significant amount of elapsed time for the sand and the glass beads. These were previously denoted as stage-2, and stage-3 respectively.

Let us consider a porous material of which the hydraulic conductivity, K indicates the following property.

$$K \gg E \quad \text{for} \quad \theta > \theta_c$$
and (22)
$$K \ll E \quad \text{for} \quad \theta < \theta_c.$$

This function is approximately satisfied for relatively uniform porous material such as the sand and glass beads employed. The hydraulic conductivity against the water content under the drying process for the porous material employed was not measured, but it is probable that θ_c is roughly consistent with the field capacity, θ_f.

(1) Stage-3

1) *Derivation of equations*

A schematic figure of water content profile in **Fig. 12** is qualitatively satisfied for the sand layer in the stage-3, and also for the Bead-3 layer, as stated in Chapter 3. It can be considered that the evaporating front at that stage moves downward through a uniform profile of water content with $\theta=\theta_c$. According to Eq. (22), the movement of liquid water in the range that $\theta_r<\theta<\theta_c$, may be represented by a horizontal flow equation where the gravitational term, K is neglected in Eq. (2). A solution to the flow equation can be given by a similarity solution as (Walker et al

(1988)[19], Ishihara et al[12], Shimojima et al[13]):

$$Z=f(\theta)\,T^{1/2} \tag{23}$$

where Z and T are shifted depth and time.

The continuity equation of liquid water in the entire domain of the porous material layer is derived as follows. By letting $\theta^* \to \theta_r$ and $\theta' \to \theta_c$ in Eq. (19), and applying Eq. (23) to the equation, we obtain

$$E=H\mathrm{d}z_e/\mathrm{d}t+(\theta_{sat}-\theta_c)\mathrm{d}z_w/\mathrm{d}t, \tag{24}$$

where

$$H=\int_{\theta_r}^{\theta_c} h\mathrm{d}\theta=const. \tag{25}$$

and

$$h(\theta)=f(\theta)/f(\theta_e)\,. \tag{26}$$

In the following analysis, we do not necessarily require the condition that $(\partial z/\partial t)_{\theta\to\theta_c-}$ in Eq. (23) be consistent with $(\partial z/\partial t)_{\theta\to\theta_c+}$.

When we define the next function,

$$r=(\mathrm{d}z_e/\mathrm{d}t)/(\mathrm{d}z_w/\mathrm{d}t), \tag{27}$$

Eq. (24) is represented by

$$E=\{H+(\theta_{sat}-\theta_c)/r\}\mathrm{d}z_e/\mathrm{d}t. \tag{28}$$

For mathematical simplicity, let us assume that r is constant. Water vapour above the evaporating front depth in the porous material layer probably satisfies Eq. (15). After eliminating z_e from Eq. (15) and Eq. (28), and solving the resulting ordinary differential equation, we obtain

$$E=G_e/\{2(t+t_0')^{1/2}\}, \tag{29}$$

where

$$G_e=[2\{H+(\theta_{sat}-\theta_c)/r\}A]^{1/2}, \tag{30}$$

with t_0' being a constant. Eq. (29) indicates that after sufficient time has elapsed, the evaporation rate begins to decrease in inverse proportion to the increase of $(t+t_0')^{1/2}$.

Substituting Eq. (29) into Eq. (15) yields

$$z_e=(2A/G_e)(t+t_0')^{1/2}-B. \tag{31}$$

And applying Eq. (31) to Eq. (27) yields

$$z_w=\{2A/(rG_e)\}(t+t_0')^{1/2}+C, \tag{32}$$

where C is a constant. Eq. (32) and Eq. (31) indicate that the water table and evaporating front depths increase with time in the characteristic manner of a similarity solution (see Eq. (23)). As the evaporation process occurs in a gravitational field, it is of interest that the similarity solutions of Eq. (29) and Eq. (32) are theoretically induced.

When the function of $h(\theta)$ defined in Eq. (26) is approximated as

$$h(\theta)=(1/r-1)\{(\theta-\theta_e)/(\theta_c-\theta_e)\}+1, \quad \text{for} \quad \theta_c>\theta>\theta_e, \tag{33}_1$$

and

$$h(\theta)=1, \quad \text{for} \quad \theta_e>\theta>\theta_r \tag{33}_2$$

the function of H (Eq. (25)) contained in Eqs. (29), (31) and (32) is represented by the next equation.

$$H=(1+1/r)(\theta_c-\theta_e)/2+(\theta_e-\theta_r). \tag{34}$$

Eq. $(33)_2$ means that the water content profile for $\theta_r<\theta<\theta_e$ is constant in shape with time.

In the cases of Bead-1 and Bead-2, it is doubtful that the observed data would satisfy the relation of Eq. (15) within the limitations of the experiment. However, if the experiment had been continued for a longer time, the relation would have certainly been satisfied. At that time, as $\theta_e=\theta_{sat}$ and $r=1$, H is given by $(\theta_c-\theta_r)$.

2) *Discussion of the experimental results*

a) *Sand*

Referring to Eq. (29), the relationship between the inverse of square of the evaporation rate, $1/E^2$, and the lapsed time, t, observed in the case of Sand K-5 at $U=$ 150 cm/s, is shown in **Fig. 20.** In this figure, the observed data (circles) of $1/E^2$

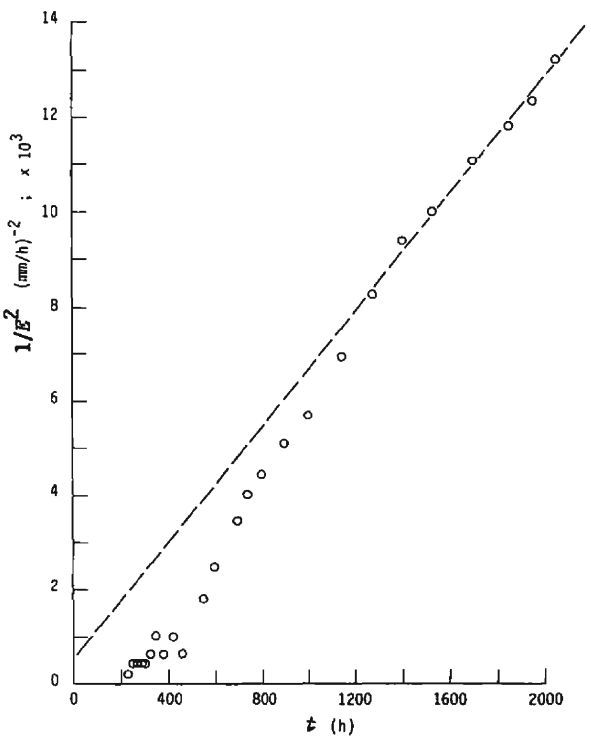

Fig. 20. Relation between $1/E^2$ and t for Sand K-5 and $U=150$ cm/s.

Table 1. Observed and calculated values of $G_e/2$ and $2A/(rG_e)$ in stage-3.

		r (—)	$G_e/2$ (mm/h$^{1/2}$)	$2A/(rG_e)$ (mm/h$^{1/2}$)
Sand K-5 (U=150 cm/s)	observed:		0.404	2.55
	calculated:	1	0.31	1.4
		0.5	0.42	2.0
Bead-3 (U=290 cm/s)	observed:		0.34	1.8
	calculated:	1	0.26	1.4

change with time, following the broken line after about 1200 h. This indicates that the change of the observed evaporation rate can be described in a similar functional form as Eq. (29), where t_0'=90 h, and a value corresponding to $G_e/2$ is given in **Table 1**.

Fig. 21 shows the relationship between the observed water table depth and a modified time, $(t+t_0')^{1/2}$, where t_0' was set equal to 90 h. In this figure, we can see that the observed water table depths (circles) changed after about 1100 h, following the broken line. The line corresponds to the functional form of Eq. (32). The starting time, 1100 h is nearly equal to the 1200 h obtained in **Fig. 20**. The value corresponding to $2A/(rG_e)$ in Eq. (32) was estimated, as shown in **Table 1**.

The calculated values of $G_e/2$, and $2A/(rG_e)$, using Eq. (8) and Eq. (16) are also shown in **Table 1**. In the calculation, by referring to **Fig. 3**, we employed 0.04, 0.06 and 0.02 as values of θ_s, θ_c, and θ_r, respectively. We assumed that the water vapour at the evaporating front was saturated, and we used observed values e.g., those for q_{atm}, q_s, and u_*. Furthermore, we took two values (1, 0.5) as r, which could not be determined a priori. In addition, the values of $G_e/2$, and $2A/(rG_e)$ were recognized to be insensitive to changes in the values of θ_e and θ_c, but sensitive to changes in r. From the Table, we can see that the calculated values of $G_e/2$, and $2A/(rG_e)$ are nearly equal to those observed when r=0.5. We could not obtain an exact value of r using

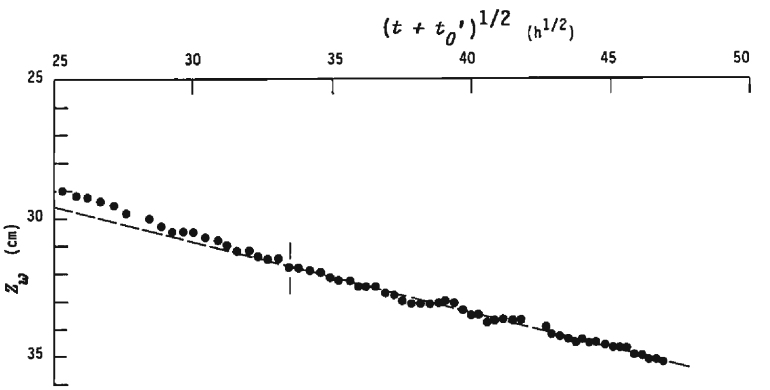

Fig. 21. Relation between z_w and $(t+t_0')^{1/2}$, corresponding to Fig. 20.

the observed data for z_w and z_e because the estimation of z_e was not sufficiently accurate, but we obtained 0.4 as an approximate value for the ratio of dz_w/dt to dz_e/dt, the r-value. This result leads us to conclude that the underlying assumption that r=const. in Eq. (29), Eq. (31) and Eq. (32) is satisfied by the experiment. It also indicates that the evaporation front moves downward with time, following to Eq. (31), and that the distance between the evaporating front and the water table increases with time.

At other wind velocities in the cases of Sand K-5 and Sand K-6, the observed data did not correspond to Eqs. (29) and (32). This is evidently based on a shorter experimental duration than that corresponding to **Fig. 20** (about three months).

b) *Bead-3*

Fig. 22 and **Fig. 23** are the same as **Fig. 20** and **Fig. 21**, respectively, but correspond to the case of Bead-3 at U=150 cm/s. In **Fig. 22**, the observed data for $1/E^2$ (circles) commences to follow the broken straight line from about 1500 h on, where t_0'=170 h. In **Fig. 23**, the observed data of z_w (circles) increase linearly with the increase of $(t+t_0')^{1/2}$. The starting time is earlier than 1500 h. Those results indicate that Eq. (29) and Eq. (32) are also satisfied in the case of Bead-3. Values corresponding to $G_e/2$ in Eq. (29) and $2A/(rG_e)$ in Eq. (32) were estimated from these figures, as in **Table 1**. The calculated values for both quantities are as follows. No BDSR-curve was obtained for Bead-3, so that the value of θ_c was not determined. Therefore, as an approximation, by setting r=1 and θ_r=0, the values of $G_e/2$ and $2A/(rG_e)$ were calculated as in **Table 1**. In comparison, it was shown that the observed values are larger than the calculated ones. The underestimation may be caused by the assumption that r=1, because the r-value is smaller than unity from

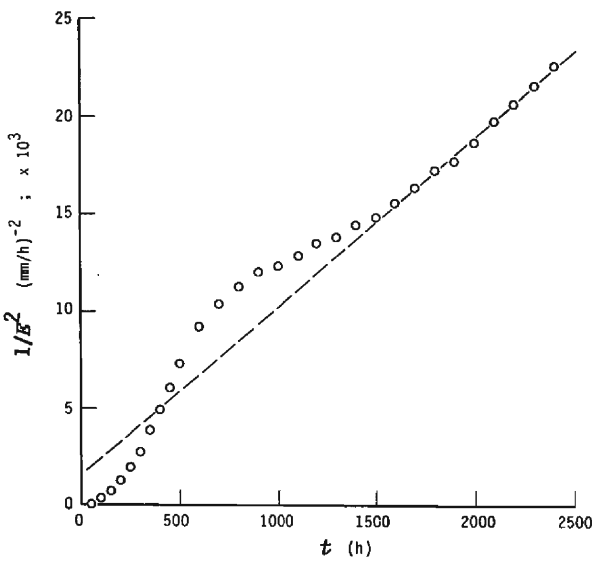

Fig. 22. Same as Fig. 20, but for the case of Bead-3 and U=150 cm/s.

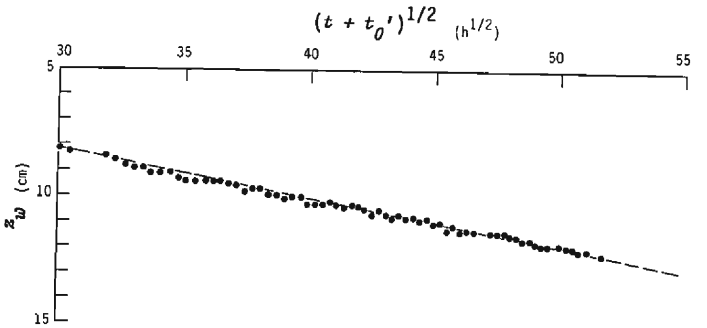

Fig. 23. Same as Fig. 21, but for the case of Bead-3 and $U=150$ cm/s.

Fig. 11 (see Chapter 3 (4) 3)).

In the case of Akadama-soil, the evaporating front hardly moved downwards, and stayed close to the surface of the layer. This situation is equivalent to the condition that $r=0$, so that Eqs. (29), (31) and (32) are not applicable for the soil layer. Evaporation under the condition that $r=0$ will be treated below.

(2) Stage-2

1) *Derivation of equations*

The evaporating front at stage-2 must be located close to the surface of porous material layers. The water content of the layers is considerable, unlike stage-3, except just below the surface of the layer. The water content at that surface, θ_0 is smaller than θ_c. Under these conditions, the first term of the right side of Eq. (19), where θ^* is replaced by θ_0, is negligibly smaller than the second term. Therefore, a continuity equation for liquid water is represented by Eq. (20), where we may consider θ' to be equivalent to θ_c.

The liquid water in a porous material layer, such as the sand obeys Eq. (1). The condition that $V_l=-E$, may be satisfied in the region where $z_e<z<z_c$. Therefore, integration of Eq. (1) leads to the next approximate equation.

$$E=K^*[(p_{wc}-p_{we})/(z_c-z_e)-1], \tag{35}$$

where p_{we} and p_{wc} are p_w at $z=z_e$ and $z=z_c$, respectively, and K^* is the hydraulic conductivity averaged between $z=z_e$ and $z=z_c$ as:

$$K^*=1\Big/\Big[\int_{z_e}^{z_c}(1/K)\mathrm{d}z/(z_c-z_e)\Big]. \tag{36}$$

When $z(\theta, t)$ for $\theta_e<\theta<\theta_c$ is given by a function in the form of variables separation, K^* is a constant. As a first approximation, let us assume that K^* is constant. Eliminating E from Eq. (20) and Eq. (35), and solving the resulting differential equation under the condition that $\mathrm{d}z_w/\mathrm{d}t \gg \mathrm{d}z_e/\mathrm{d}t$ yields

$$K^*(t-t_0)/(\theta_{sat}-\theta_c)=Y-(p_{wc}-p_{we})\ln Y, \tag{37}$$

where

$$Y=p_{wc}-z_c-p_{we}+z_e,$$

$$t_0=t_0''-(\theta_{sat}-\theta_c)\{Y_0''-(p_c-p_e)\ln Y_0''\}/K*$$

and Y_0'' is Y at $t=t_0''$ (=const.). In addition, the condition that $dz_w/dt \gg dz_e/dt$ is included in Eq. (20). In a comparison of the magnitudes of θ_e and θ_c, the matrix potential, p_{we} (<0) at $z=z_e$ must be much smaller than p_{wc}. Thus, the right side of Eq. (37) becomes:

$$Y-(p_{wc}-p_{we})\ln Y=-(p_{wc}-p_{we})\ln Y. \tag{38}$$

Applying Eq. (38) to Eq. (37), and rearranging the resulting equation yields

$$z_w=-\exp\{-f(t-t_0)\}+p_{wc}-p_{we}+z^{(wc)}+z_e, \tag{39}$$

where

$$f=K*/\{(\theta_{sat}-\theta_c)(p_{wc}-p_{we})\} \tag{40}$$

and $z^{(wc)}$ is z_w-z_c (=const.). Since the value of z_e has been assumed to be small, the sum of the second, third, and fourth terms on the right side of Eq. (39) becomes a constant. Therefore, the water table depth increases with time as an exponential function of time.

Substituting Eq. (39) into Eq. (20) yields

$$E=(\theta_{sat}-\theta_c)f\exp\{-f(t-t_0)\}. \tag{41}$$

Eq. (41) indicates that the evaporation rate decreases exponentially with time.

By eliminating the exponential function from Eqs. (39) and (41), we obtain the next equation.

$$E=nz_w+m, \tag{42}$$

where

$$n=f(\theta_{sat}-\theta_c) \tag{43}$$

and

$$m=f(\theta_{sat}-\theta_c)\{p_{wc}-p_{we}+z^{(wc)}+z_e\}. \tag{44}$$

Eq. (42) suggests that the evaporation rate decreases linearly with increasing water table depth.

2) *Examination of the experimental data*

a) *Values of f_*, f_{**} and θ_c*

Sand:

As stated in Chapter 3, it was experimentally determined that the evaporation rate in the cases of Sand K-5 and Sand K-6 decayed exponentially, as described by Eq. (41) for a certain duration (T_e). The values of the coefficient of the exponential decay are shown in **Table 2**.

Figs. 24(a) and **(b)** show the time changes of the derivative of the water table depth with respect to time, dz_w/dt, in logarithmic scale for Sand K-5 and Sand K-6, respectively, where dz_w/dt was represented by the mean slope of z_w over an interval of a time. In these figures, the observed data decrease with time, forming the broken

Table 2. Characteristic values in stage-2.

	U (cm/s)	f_* (l/h)	f_{**} (l/h)	θ_c (—)	n (l/h)
Sand K-5	150	0.0093	0.0090	0.14	0.0030
	290	0.0105	0.0098	0.10	0.0044
Sand K-6	215	0.0021	0.0048	0.20	0.00109
	285	0.0067	0.0068	0.20	0.00153
	295	0.0088	0.0082	0.09	0.00313
Akadama-soil	290	0.0022	0.0022	0.164	0.00107

line for a certain time (T_w), so that the result reveals the fact that the water table depth increases with time in a functional form similar to Eq. (39). Comparison of T_w and T_e leads to the result that both intervals are consistent with each other (see **Figs. 1** and **7**). Values of the slopes of the broken lines, f_{**}, are also summarized in **Table 2**.

Comparing f_{**} with f_* in **Table 2**, we can see that the values of both quantities are nearly equal to each other except at $U=215$ cm/s. The value of θ_c contained in Eqs. (39) and (41) can be evaluated using the observed values of n and f_* or f_{**}. The calculated values are also given in **Table 2**, where θ_{sat} is 0.46 for both sands. It was shown that the value of θ_c was larger than that of the field capacity, but it was nearly equal to the value of the water content at which the BDSR-curve shows an inflexion point, as stated in Section 2 (1). The calculated water content is obviously larger than θ_e, as seen in **Fig. 3** for Sand K-5. The hydraulic conductivity under the drying process was not measured as stated before, but was expected to change abruptly around at $\theta=\theta_c$, similar to the step-wise function given by Eq. (22). Although the

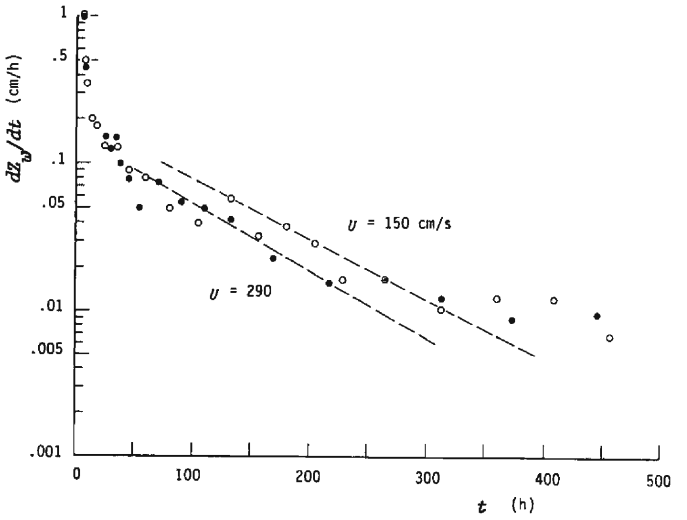

(a) in the case of Sand K-5.

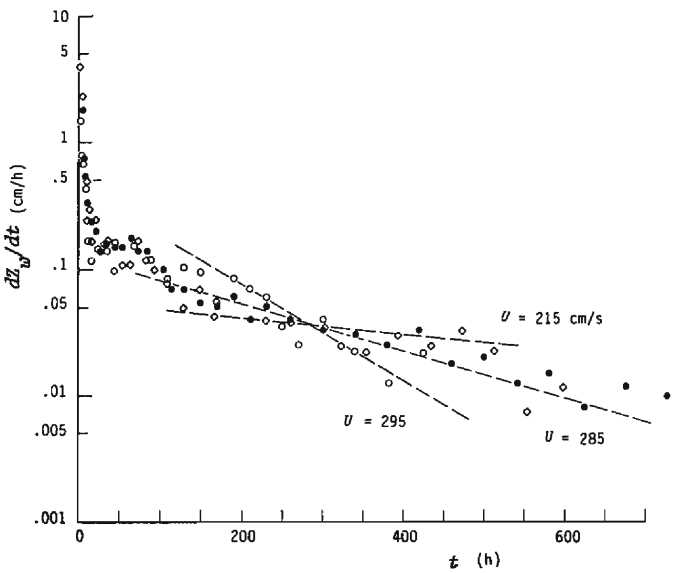

(b) in the case of sand K-6.

Fig. 24. Changes of dz_w/dt with time.

values of θ_c calculated for the sand layers are not consistent with the field capacity, the results obtained above are not unreasonable. It follows that the observed quantities, f_* and f_{**}, are equivalent to f defined in Eq. (40).

In Section 2(1) we defined the W-range and the S-range in terms of the evaporation rate and the water table depth. The f defined in Eq. (40) at stage-2 must be constant, regardless of the wind velocity, because K^*, $p_{wc}-p_{we}$ and θ_c are expected to be constant. However, the values of f_* or f_{**} corresponding to f were in fact dependent on the applied wind velocity, though these fluctuations were not large in magnitude. As a result, stage-2 is still included in the W-range, and is affected by the friction velocity related to water vapour transfer in the atmospheric turbulent boundary layer.

Akadama-soil:

In the case of Akadama-soil the change in dz_w/dt with time is shown in **Fig. 8**, and the relationship between E and z_w for the same time is shown in **Fig. 15**. These experimental results indicated the following. With the exception of the very first stage of the experiment, the time-changes in the evaporation rate and water table depth follow the functional forms of Eq. (41) and Eq. (39), respectively. The linear relation between E and z_w shown in Eq. (42) is satisfied. The values of f_{**} and f_* (**Fig. 8**) are shown in **Table 2**. The θ_c-value for this soil can be estimated in the same manner as for the sands, and the result shown in **Table 2** indicates that the value is consistent with the field capacity which is determined mainly by properties of the micropores. The validity of the present results is based on the fact that the evaporating front in

practice always remained near the exposed surface and which further supports the theoretical development in 1) as being reasonable.

b) *Functional form of $E(t)$*

According to previous research on the drying of initially wetted soil profiles which do not contain a water table anywhere near enough to the soil surface to have any bearing on the evaporation process (Hillel[3], Clapp (1983)[20),21)]), in the falling-rate (second) stage following the constant-rate (first) stage, evaporation rate is said to decrease in the manner expressed by Eq. $(45)_1$ to be derived below. When the gravity term in Eq. (1) or Eq. (35) is negligibly smaller than the water pressure term in the range where $\theta_e<\theta<\theta_c$, by directly omitting unity in $[\cdot\cdot]$ of the right side of Eq. (35), we obtain

$$E=\text{const.}/(t+\text{const.})^{1/2} \tag{45}_1$$

and

$$z_w=\text{const.}\,(t+\text{const.})^{1/2}+\text{const.} \tag{45}_2$$

Following Eq. $(45)_1$, and plotting the observed data of $1/E^2$ against t for the sand yielded a linear relation between both quantities over a short duration, but the duration was much shorter than T_e defined in a). In the derivation for Eqs. (39), (41) and (42), we had to introduce the assumption that $K^*=$const. and an approximate equation of Eq. (38), though some of them was not necessarily verified directly. In spite of such limitations, the derived form of Eq. (41) is more applicable than Eq. $(45)_1$.

For the sand layer, the evaporation equation may be roughly represented as follows.

$$\begin{aligned} &E=E_{pot}; && t<t_a\text{(stage-1)} \\ &E=E_{pot}(t_a)\exp\{-f(t-t_a)\}; && t_a<t<t_b\text{(stage-2)} \qquad (41) \\ &E=(G_e/2)/(t+t_0')^{1/2}; && t>t_c\text{(stage-3)} \qquad (29) \end{aligned}$$

where E_{pot} is a function of temperature at $z=0$ and in proportion to u_*, and t_a, t_b and t_c are each constant. However, the equation for $t_b<t<t_c$ is still undetermined. A further problem is how to determine the evaporation equation for $t_b<t<t_c$ using the equations for $t_a<t<t_b$ and $t>t_c$.

5. Conclusions

Evaporation process from bare land like a desert with an unrestricted underlying water table has been explored through a laboratory experiment where a turbulent wind was continuously applied to a layer consisting of one of several kinds of porous materials, paying particular attention to the effect of the turbulent wind on evaporation. The following has been elucidated.

1) The turbulent wind affects the evaporation rate with the degree becoming smaller with increasing depth of the water table, and accompanied by downward advancement of the evaporating front. This effect due to the wind increases, as the pore-size of the porous material in a layer is larger.

2) While the effect of turbulent diffusion is dominant on the water vapour transfer in the porous material layers, E/u_* is uniquely determined by z_w regardless of wind velocity.

3) Time-courses of the evaporation rate and the water table depth respectively show a characteristic change for a particular duration. In the cases of the sand and Akadama-soil layers, at the second stage following the first stage, the evaporation rate and the water table depth change with time in an exponential manner represented by Eq. (41) and Eq. (39), respectively. These changes persist for a very long time for Akadama-soil layer with its double pore structure because the evaporating front always stays near the surface of the layer.

4) After a significant amount of time has elapsed, in the cases of the sand and the glass bead with a relatively small particle-diameter (on the order of 1 mm, Bead-3), time courses of the evaporation rate, the water table and the evaporating front depths are given by a similarity solution from Eq. (29), Eq. (32) and Eq. (31), respectively. As an example, for Sand K-5, the ratio of moving velocity of the evaporating front to that of the water table was about 0.5.

Acknowledgments

The authors wish to thank Mr. Yasuhisa Kuzuha, Mr. Yujin Minobe and Mr. Hiroshi Harada for their aid in the experiment and for their valuable discussion.

References

1) Sadler, B. S. and W. E. Cox: Water management: the socio-political context, Nature and Resources, Vol. XXII, No. 3, UNESCO, 1986, pp. 12–19.
2) Brutsaert, W. H.: Evaporation into the atmosphere, Reidel Pub. Comp., 1982.
3) Hillel, D.: Applications of soil physics, Academic Press, 1980.
4) Camillo, P. L., R. J. Gurney and R. H. Schmugge: A soil and atmosphere boundary layer model for evapotranspiration and soil moisture studies, Water Resou. Res., Vol. 19, 1983, pp. 371–380.
5) Bristow, K. L., G. S. Campbell, R. I. Papendick and L. F. Elliott: Simulation of heat and moisture transfer through a surface residue-soil System, Agr. and Forest Meteorol., Vol. 36, 1986, pp. 193–214.
6) Kuzuha, Y., Y. Ishihara and E. Shimojima: A numerical simulation on the evaporation in a bare land, —In the case of a restricted groundwater table—, Annuals, Disas. Prev. Res. Inst., Kyoto Univ., Vol. 31 B-2, 1988, pp. 161–180 (in Japanese).
7) Ishihara, Y., Y. Kuzuha and E. Shimojima: A numerical simulation on the evaporation in bare land (2), —Effect of Time-variation of wind speed on the evaporation—, Annuals, Disas. Prev. Res. Inst., Kyoto Univ., No. 32 B-2, 1989, pp. 297–308 (in Japanese).
8) Nakano, M.: Soil water movement during the first stage of drying of a moist sandy soil under a very low drying rate, Soil Sci., Vol. 124, 1977, pp. 67–72.
9) Barnes, C. J. and G. B. Allison: The distribution of deuterium and ^{18}O in dry soils, 1. Theory, J. Hydrol., Vol. 60, 1983, pp. 141–156.
10) Barnes, C. J. and G. B. Allison: The distribution of deuterium and ^{18}O in dry soils, 3. Theory for non-isothermal water movement, J. Hydrol., Vol. 79, 1984, pp. 119–135.
11) Allison, G. B., C. J. Barnes and M. W. Hughes: The distribution of deuterium and ^{18}O in dry soils, 2. Experimental, J. Hydrol., Vol. 64, 1983, pp. 377–397.
12) Ishihara, Y., E. Shimojima and H. Harada: On the evaporation from bare land with an underlying restricted water table, Annuals, Disas. Prev. Res. Inst., Kyoto Univ., Vol. 32 B-2, 1989, pp. 281–295

(in Japanese).
13) Shimojima, E., A. A. Curtis and J. V. Turner: The mechanism of evaporation from sand columns with restricted and unrestricted water tables using deuterium under turbulent airflow conditions, J. Hydrol., (submitted).
14) Philip, J. R. and D. A. de Vries: Moisture movement in porous materials under temperature gradient, Tran. Am. Geophy. Un., Vol. 38, 1957, pp. 222–228.
15) Farrell, D. A., E. L. Greacen and C. G. Gurr: Vapour transfer in soils due to air turbulence, Soil Sci., Vol. 102, No. 5, 1966, pp. 305–313.
16) Scotter, D. R. and P. A. C. Raats: Dispersion of water vapour in soils due to air turbulence, Water Resou. Res., Vol. 108, No. 3, 1969, pp. 170–176.
17) Ishihara, Y., E. Shimojima and Y. Minobe: Water vapour transfer in evaporation from a bare land, Proc. the 6th Congress Asia & Pacific Regional Div. of Internat. Assoc. Hydraul. Res., Vol. 1, 1988, pp. 33–40.
18) Philip, J. R.: On solving the unsaturated flow equation, 1, The flux-concentration relation, Soil Sci., Vol. 116, 1973, pp. 328–335.
19) Walker, G. R., M. W. Hughes, G. B. Allison and C. J. Barnes: The movement of isotopes of water during evaporation from a bare soil surface, J. Hydrol., Vol. 97, 1988, pp. 181–197.
20) Clapp, R. B.: The desorptivity model of bulk soil-water evaporation, AgRISTARS Report, Lyndon B. Johnson Space Center, 1983.
21) Clapp, R. B.: The continuous similarity model of bulk soil-water evaporation, AgRISTARS Report, Lyndon B. Johonson Space Center, 1983.